Cellular and Molecular Life Sciences (2025) 82:117
https://doi.org/10.1007/s00018-025-05616-w

ORIGINAL ARTICLE

Loss of *Cep135* causes oligoasthenoteratozoospermia and male infertility in mice

Hui Liu[1,2] · Haozheng Zhang[3] · Guanghao Qin[1] · Tingting Song[1] · Xin Liu[1] · Zongzhuang Wen[6] · Min Liu[4,5] · Xianmei Wang[6] · Xiaolong Fu[1,2,7] · Jiangang Gao[6]

Received: 21 October 2024 / Revised: 10 January 2025 / Accepted: 4 February 2025

Abstract

Centrosomal proteins (Cep), as crucial scaffolding molecules, play a pivotal role in the biogenesis of centrioles and the regulation of the cell cycle. To date, mutation in *Cep135* has been reported to be closely associated with multiple morphological abnormalities of the flagella (MMAF) in humans. However, the specific mechanism of *Cep135* in spermatogenesis and its detailed role in male infertility remains largely unexplored. In this study, we present compelling evidence that *Cep135* functions as a pathogenic gene responsible for oligoasthenoteratozoospermia (OAT) and male infertility in mice. By selectively deleting *Cep135* in premeiotic germ cells using *Stra8*-Cre mice crossed with *Cep135*$^{flox/flox}$ mice, we observed that *Cep135* knockdown produced abnormal sperm morphology, germ cell apoptosis and consequentlybecame complete infertility, but did not impact premeiosis. Scanning and transmission electron microscopy revealed defects in acrosome, flagellum, and head-to-tail connections during spermatogenesis. Proteomic analysis further indicated that CEP135 deletion led to a significant reduction in proteins mainly associated with acrosome formation, sperm heads, sperm flagellum and microtubule assembly. Additionally, CEP135 interacts with spermatogenic proteins SPATA6 and AKAP3, regulating their expression and stability. Deficiency in CEP135 or its interacting proteins resulted in ciliary shortening. In conclusion, our study profoundly unveils the central role of *Cep135* in spermatogenesis and male fertility. This discovery not only deepens our comprehension of spermatogenesis but also furnishes a solid theoretical foundation and experimental evidence that can guide the formulation of therapeutic and preventive strategies for male infertility.

Keywords Male infertility · Spermatogenesis · Oligoasthenoteratozoospermia · Sperm · Mouse model

Abbreviations

3-NT	3-Nitrotyrosine
4-HNE	4-Hydroxynonenal
CASA	Computer-Assisted Sperm Analysis
CCDC	Coiled-Coil Domain Containing
CEP	Centrosomal Protein
CFAP	Cilia and Flagella Associated Protein
CHX	Cycloheximide

✉ Min Liu
Justdoit.66@163.com

✉ Xianmei Wang
wangxianmei0123@126.com

✉ Xiaolong Fu
fuxiaolong@sdfmu.edu.cn

✉ Jiangang Gao
jggao@sdu.edu.cn

[1] Department of Histology and Embryology, School of Clinical and Basic Medical Sciences, Shandong First Medical University & Shandong Academy of Medical Science, Jinan, Shandong, China

[2] Medical Science and Technology Innovation Center, Shandong First Medical University, Jinan, Shandong, China

[3] Children's Hospital Affiliated to Shandong University, Jinan, Shandong, China

[4] The Affiliated Taian City Central Hospital of Qingdao University, Taian, China

[5] School of Basic Medical Sciences, Shandong University, Jinan, Shandong, China

[6] Central Hospital Affiliated to Shandong First Medical University, Jinan, Shandong, China

[7] Shandong Provincial Hospital Affiliated to Shandong First Medical University, Jinan, Shandong, China

Published online: 17 March 2025

co-IP	co-Immunoprecipitation
CP	Capitulum
DSBs	Double Strand Breaks
HIPK4	Homeodomain-Interacting Protein Kinase 4
HTCA	Head-to-Tail Connecting Apparatus
MFSD6L	Major Facilitator Superfamily Domain-containing Protein 6-like
MMAF	Multiple Morphological Abnormalities of the Flagella
OAT	Oligoasthenoteratozoospermia
ODF	Outer Dense Fiber
PCNA	Proliferating Cell Nuclear Antigen
PNA	Lectin Peanut Agglutinin
POC1B	Proteome of Centriole 1 Centriolar Protein B
PC	Proximal Centriole
PPIs	Protein-Protein Interactions
ROS	Reactive Oxygen Species
SC	Segmented Column
TEM	Transmission Electron Microscopy
VAP	Average Path Velocity
VCL	Curve Linear Velocity
VSL	Straight Linear Velocity

Introduction

Clinical infertility affects 10–20% of couples globally, constituting a significant public health concern [64], with male factors accounting for approximately half of these cases [53]. Male infertility often manifests as reduced sperm count (azoospermia or oligospermia), decreased sperm motility (asthenospermia), abnormal sperm morphology (teratospermia), or a combination of these symptoms, collectively termed OAT [4], which is characterized by abnormal sperm count, motility, and morphology, contributes to one-fifth of male infertility cases and is typically caused by abnormal spermatogenesis [60].

Spermatogenesis is a complex, multi-step process involving spermatogonia mitosis, spermatocyte meiosis, and haploid sperm maturation within the testicular spermatogenic epithelium. Disruptions in this intricate process lead to male infertility [1, 7, 15]. Numerous factors, including endocrine disorders [41], metabolic abnormalities [40], environmental toxicants [42], oxidative stress [48], heredity factors [33], obesity [3] can adversely affect spermatogenesis and male fertility. Notably, genetic mutations are implicated in up to 50% of male infertility cases, with growing evidence highlighting their association with the condition [4, 20, 33, 36].

There is a growing body of evidence suggesting a correlation between genetic mutations and OAT, particularly involving genes belonging to the coiled-coil domain-containing (CCDC) family, CEP family, cilia and flagella associated protein (CFAP) family, as well as other genes such as proteome of centriole 1 centriolar protein B (POC1B), homeodomain-interacting protein kinase 4 (HIPK4), and major facilitator superfamily domain-containing protein 6-like (MFSD6L), which have all been reported to be associated with male infertility [11, 12, 24, 25, 30, 46, 68, 69]. Intriguingly, these genetic mutations primarily manifest in phenotypes like MMAF, abnormal head-tail connections, acrosomal deformities, and mitochondrial sheath abnormalities. In summary, the precise identification of candidate genes and specific phenotypes associated with OAT will substantially enhance our understanding of the underlying pathogenesis of this conditon and lay a solid foundation for advancing related therapeutic strategies.

The centrosome, a eukaryotic organelle, comprises a pair of nine symmetrical microtubules organized into a cylindrical centriole surrounded by pericentriolar material [16], which is involved in a variety of biological processes, including cell division, cell migration, cilia formation [8]. Defects in centrosomes have been linked to diseases such as microcephaly, ciliopathies, and cancer [28, 39, 45]. In male reproductive system, centrosomes are crucial for sperm flagella development and head-tail junction, thereby playing a pivotal rolein male fertility [5]. Despite the centrosome being composed of hundreds of proteins, the precise mechanisms underlying their roles in male reproduction remain unclear. Previous studies have highlighted the functional deficits of various CEP family members in spermatogenesis. For instance, the functional deficiency of *Cep78* e reulted in multiple morphological abnormalities of sperm flagella, low sperm count and sperm motility, it eventually led to male sterility in both humans and mice [67, 70]. Cep128knockout displayed damaged flagella and male sterility associated with impaired sperm quality [66]. Loss of *Cep70* caused abnormal development of sperm flagella and acrosome in mice [37, 46], while it has been reported that overexpression of *Cep55* inhibits *Foxo1* nuclear retention through continuous activation of PI3K/Akt signaling pathway, thus leading to male specific sterility in mice [51]. And loss of *Cep63* caused severe damage to meiosis recombination, resulting in male sterility [38]. Deletion of *Cep131* generated damage to manchette structure and flagella, leading to sterility [22]. Additionally, *Cep164*, *Cep192*, *Cep250*, and the interaction between *Cep350* and *Cfap157* have also been implicated in male sterility [17, 21, 23, 58].

CEP135, a core centrosomal protein with a coiled domain, stabilizes centrioles by interacting with their sidewalls and/or microtubule walls [32]. CEP135 serves as a scaffold during centriole biogenesis and regulates centriole replication [13, 31]. It is essential for the integrity of centriole structure in proliferating cells and limits centrosome expansion in S-phase-blocked cells [27]. In humans, CEP135 truncating

mutations have been associated with primary microcephaly and centrosome dysfunction [26]. The disorder of *Cep135* isomer facilitates centrosome expansion in breast cancer cells [18]. Moreover, in Drosophila, *Cep135* is a conserved component involved in centriole and flagellar biogenesis, where it binds and stabilizes microtubules, playing a crucial role in the initial stages of central microtubule formation [10]. In summary, these studies underscore the necessity of *Cep135* for maintaining the structural integrity and replication of centrioles. In the reproductive system, sperm centrosomes exhibit specialized features, comprising a proximal centriole resembling a barrel, a distal centriole shaped like a funnel, and pericentriolar material forming a striated (or segmented) column [54]. A previously documented case of a homozygous *Cep135* mutation (p.D455V) was found to cause severe human MMAF, resulting in a scarcity of normal sperm and a mass of sperm with abnormal flagellum morphology. Despite undergoing intracytoplasmic sperm injection (ICSI) and embryo transfer, conception was not achieved, ultimately leading to infertility. However, the exact function and mechanism of Cep135 in spermatogenesis and male infertility remain elusive [49]. The present study endeavors to systematically explore the precise functions and roles of *Cep135* in the male reproductive process through meticulously constructed animal models.

To elucidate the functional role of *Cep135*, a conditional knockout mouse model targeting *Cep135* was generated using *Stra8*-Cre mice, enabling specific knockout of *Cep135* in premeiotic germ cells. This deletion of *Cep135* resulted in defective acrosome formation, abnormally elongated manchette structures, irregularities in flagellar structure, and disrupted head-to-tail connections. Consequently, male *Cep135* conditional knockout (cKO) mice exhibited infertility due to impaired spermatogenesis.

Materials and methods

Animals

All experimental protocols involving animals were granted approval by the Ethics Committee of Shandong First Medical University (Approval Number: W202211250348, Jinan, China), ensuring strict adherence to Chinese animal protection laws and regulations. The generation of *Cep135*$^{flox/flox}$ mice was achieved through CRISPR/Cas9 technology and targeted homologous recombination. The Two single guide RNAs (sgRNAs) were designed to target exons 3 and 4 of Cep135, and the constructed sgRNAs and Cas9 mRNA were co-injected into fertilized eggs, which were then transplanted into pseudopregnant female mice to generate targeted conditional knockout offspring. The Founder mice (F0) generation was identified by polymerase chain reaction (PCR) and crossed with wild-type (WT) mice to detect germline transmission. PCR analysis revealed the insertion of loxP in the F1 and F2 generations. To generate the germ cell-specific knockout of *Cep135*, *Cep135*$^{flox/flox}$ and *Cep135*$^{flox/+}$ mice were crossed with *Stra8*-Cre mice. *Cep135*$^{flox/flox}$, Cre(−) mice or *Cep135*$^{flox/+}$, Cre(−) mice, termed as wild type mice, were used as controls in all experiments. All mice were maintained on a consistent C57BL/6J genetic background and housed in environmentally controlled conditions, with unlimited access to food and water, under a regulated 12-hour light/dark cycle.

Genotyping

Genomic DNA, extracted from mouse feet, underwent PCR amplification in a thermal cycler (Applied Biosystems VeritiPro, Thermo Fisher Scientific, USA). To genotype *Cep135* knockout mice, specific primers were employed to distinguish between the control and *Cep135* conditional knockout (cKO) alleles: 5'-TGCTAACTCATTTTGTTGAGTGCC-3' (forward) and 5'-ATCAAAGGGTCCTCAAGTTTCTCA-3' (reverse). The PCR protocol was as follows: an initial denaturation step at 95°C for 3 minutes, followed by 35 cycles of 95°C for 30 seconds (denaturation), 60°C for 30 seconds (annealing), and 72°C for 30 seconds (extension), with a final extension step at 72°C for 3 minutes.Similarly, for genotyping *Stra8*-Cre mice to assess Cre recombinase activity, a separate set of primers was used: 5'-TCGATGCAACGAGTGATGAG-3' (forward) and 5'-TTCGGCTATACGTAACAGGG-3' (reverse). The PCR conditions for *Stra8*-Cre genotyping mirrored those for *Cep135*, with an initial denaturation at 95 °C for 3 min, 35 cycles of 95 °C for 30 s, 60 °C for 30 s, and 72 °C for 30 s, followed by a final extension at 72 °C for 3 min. The PCR products were then analyzed using 1.5% agarose gel electrophoresis.

Fertility assessment, sperm count and casa analysis

To assess fertility, male mice of approximately 2 months old, including both control and conditional knockout groups, were each paired with two randomly selected adult wild-type females. Over a period of at least 3 months, the pregnancy rate and the total number of offspring produced were meticulously recorded. Subsequently, sperms were collected from the epididymides and incubated in PBS solution at 37 °C. The sperm samples were then appropriately diluted for further analysis. Sperm motility, including both total and progressive motility, was quantitatively assessed using computer-assisted semen analysis (CASA). Following this, the incubated sperm solution was further diluted at a ratio of 1:100, and the sperm count was determined using

a hemocytometer. Statistical analysis of the data was performed using unpaired T-tests with equal standard error of the mean (SEM) in GraphPad Prism 9 software.

Antibodies

The primary and secondary antibodies utilized, along with their respective dilutions, are detailed in Table S1.

Western blotting

For the preparation of total protein extracts from testes, the tissue was finely ground using a low-temperature homogenizer (KZ-III-F, Servicebio) in 400 µl of RIPA buffer supplemented with a protein phosphatase inhibitor cocktail (P1260, Solarbio, China), adhering strictly to the manufacturer's instructions (89900, Thermo Fisher Scientific, USA). The homogenized tissue was allowed to stand on ice for 15 min, followed by centrifugation at 13,000 rpm for 15 min at 4 °C. The resulting tissue or cell extracts were boiled for 10–15 min and then subjected to SDS-PAGE electrophoresis. Subsequently, the proteins were transferred onto polyvinylidene difluoride membranes (IPVH00010, Millipore, USA). After a 30-minute incubation in fast blocking buffer (PS108P, EpiZyme, China), the membranes were incubated with the primary and secondary antibodies diluted in antibody diluent (36206ES76, Yeasen, China). Finally, the membranes were scanned using an enhanced chemilumines image analysis system (Tanon 5200 multi, China), with the specific antibodies listed in Table S1.

Histological analysis of testis and epididymis

The testes and epididymides were initially fixed in Bouin's solution overnight at 4 °C. Following thorough washing in phosphate-buffered saline (PBS), the testes underwent a dehydration process involving gradual concentrations of ethanol and xylene, followed by embedding in paraffin. Sections of 4 µm thickness were then cut and mounted onto microscope slides using standard procedures. After deparaffinization and rehydration, the tissue sections were stained with haematoxylin and eosin (H&E) for histological examination, and the slides were visualized using an Olympus microscope (BX53, Japan).

TUNEL assays

For apotosis staining, apoptotic cells were analysed by terminal deoxynucleotidyl transferase-mediated dUTP-biotin nick end labeling (TUNEL) assay, which was performed with the TUNEL Kit (C1088, Beyotime, China) following the manufacturer's instructions. Fluorescence images were captured using a fluorescence microscope (OLYMPUS, BX53, Japan).

PNA and PAS staining

The outer acrosomal membrane of spermatids was detected using Peanut agglutinin (PNA), while acrosomal sugars were stained with periodic acid-Schiff (PAS). Following deparaffinization and rehydration, the tissue sections were incubated with fluorescein isothiocyanate (FITC)-conjugated PNA (#L7381, 1:1000, Sigma Aldrich, Germany) for 30 min at 37 °C to label the outer acrosomal membrane. PAS staining was then performed on the testes sections using the PAS Stain Kit (#G1280, Solarbio, China), adhering to the manufacturer's protocol.

Histological and immunofluorescence analysis of spermatozoa

A small incision was delicately made on the isolated tail of the epididymis, positioned within the orifice plate containing PBS. The sperm was then allowed to swim out by incubating in an incubator maintained at 37 °C for 15 min. Subsequently, 10 µl of the sperm suspension were applied onto an adhesive slide, which was then aired and left to dry for 2 h. The slide was fixed with 4% paraformaldehyde for 30 min. Following this, either conventional hematoxylin-eosin staining (HE) staining methods were employed or, after thorough washing three times with 1x PBS, the slide was immersed in fresh 1x PBS containing 0.1% Triton X-100 for 30 min at room temperature for permeabilization. This was followed by incubation in 5% bovine serum albumin for 60 min at room temperature to block non-specific binding sites. The samples were then incubated overnight at 4 °C with primary antibodies, followed by a 1-hour incubation at 37 °C with secondary antibodies and counterstaining with 4'6-diamidino-2-phenylindole (DAPI) (H120010, Vectorlabs). Images were captured using a confocal microscope (Olympus, BX53).

Immunofluorescence of testicular tissue

For testicular tissue staining, paraffin sections of the testis underwent dewaxing and rehydration procedures. The sections were then subjected to antigen retrieval by boiling in sodium citrate buffer (#C1032, Solarbio, China) for 20 min, followed by three washes in PBS. Blocking was achieved using 5% goat serum for 30 min, and the sections were then incubated overnight at 4 °C with primary antibodies. After washing, the slides were incubated with secondary antibodies for 1 h at 37 °C, followed by incubation with 4',6-diamidino-2-phenylindole (DAPI). It is noteworthy

that all steps subsequent to the addition of the secondary antibody were performed under light-protected conditions.

Transmisson electron microscopy (TEM)

Testicular tissue was promptly harvested from both control and *Cep135* cKO male mice. The tissue was initially prefixed with 3% glutaraldehyde and postfixed in 1% osmium tetroxide. It was then dehydrated through a graded series of acetone, infiltrated with Epox 812, and embedded. Semithin sections were stained with methylene blue, whereas ultrathin sections, obtained using a diamond knife, were stained with uranyl acetate and lead citrate. Finally, these sections were examined under a JEM-1400 Flash transmission electron microscope.

Scanning electron microscopy (SEM)

Samples were fixed with 2.5% glutaraldehyde in 0.1 M sodium cacodylate (pH 7.2) for 1 h, then dehydrated using progressive ethanol concentrations (35, 50, 75, 90, 95, and 100%) for 10 min's each and dried using a CO2 critical-point dryer (Eiko HCP-2, Hitachi). Finally, the samples were observed under the SEM (Hitachi S3400) at an accelerating voltage of 15 kV.

Isolation of the testicular germ cells

Testes were harvested promptly in ice-cold PBS, and the tunica albuginea was meticulously removed. The testicular tissue was then minced in 200 µl of a digestion medium until complete digestion of the seminiferous tubules was visually confirmed. Subsequently, 800 µl of the remaining digestion medium was added, and the mixture was incubated for 25 min at 37 °C with slow, continuous rotation. Additional mechanical disruption was achieved by pipetting the solution five times using wide-bore pipette tips. The resulting suspension was filtered through a 35 µm pore size filter to obtain a single-cell suspension. Care was taken to pipette the suspension slowly to prevent clogging and cell damage. The cells were collected by centrifugation at 400 g for 10 min at 37 °C. The supernatant was discarded, and the cell pellet was resuspended in an appropriate volume of PBS. Subsequently, 4% paraformaldehyde (PFA) solution was added to the cell suspension, and 20 µl of this mixture were dropped onto a slide. The slide was air-dried at room temperature for 2 h, followed by immunofluorescence staining using conventional methods.

siRNA knockdown and rescue

Scramble-siRNA, *Cep135*-siRNA were purchased from Sangon biotechnology (Sangon, Shanghai, China) with their respective sequences detailed in Table S2. Cep135^{syn}-HA constructs were specifically designed to harbor synonymous mutations within the siRNA-targeting sequence, thereby evading siRNA-mediated knockdown (Table S2). Both siRNAs and rescue plasmids were transfected using siRNA-mate (GenePharma, Shanghai, China) according to the manufacturer's protocol.

Cell culture and transient transfection

HEK293T cell lines were purchased from Procell (CL-0005, 1×10^6 cells, Wu han, China) and maintained in Dulbecco's Modified Eagle Medium (DMEM, 11965092, Gibco), supplemented with 10% fetal bovine serum (FBS, FSP500, Excell) in an incubator set at 37 °C with 5% CO2. The expression plasmids encoding *Cep135* (NM_199032) and inserted into HA-tagged pCMV vectors (pcDNA3.1-HA-C) were constructed by Keyybio (Shandong, China) according to the manufacturer's instructions. Full-length cDNAs encoding *Spata6*, *Akap3* were amplified by PCR using mouse testis cDNA as the template and cloned into Myc-tagged pCMV vectors. The construction of expression plasmids in this study was confirmed by sequencing (Sango Biotech). The plasmids were transient transfected with Lipofectamine 3000 (L3000015, Invitrogen) for cell lines according to the manufacturer's protocol. Following transfection, cells were allowed to incubate for 48 h before being harvested. The cycloheximide (CHX) used in protein degradation analysis was purchased from MedChemExpress (MCE, Shanghai, China).

Proteomic analysis

Testicular tissue for proteomic analysis was obtained from 2 months-old C57BL/6 male mice and subjected to LC-MS/MS analysis with a standard protocol. In brief: (1) The mouse testes were finely powdered using liquid nitrogen and promptly transferred to chilled tubes containing lysis buffer enriched with 1% Protease Inhibitor Cocktail. The homogenate was then sonicated with a high-intensity ultrasonic processor (Scientz) to facilitate lysis. Following centrifugation, the supernatant was carefully collected, and the protein concentration was accurately determined; (2) Subsequently, the proteins underwent trypsin digestion and purification. The resulting peptides were resuspended in 0.5 M Tetrathylammonium bromide (TEAB) and prepared for labeling according to the manufacturer's instructions using the Tandem mass tag (TMT) kit; (3) The labeled peptides were then

subjected to LC-MS/MS identification and quantification on a state-of-the-art Thermo Scientific Q ExactiveTM HF-X mass spectrometer (Thermo Fisher Scientific), equipped with a nano-electrospray ion source, ensuring precise and sensitive analysis; (4) The raw mass spectrometry data were meticulously processed using a range of bioinformatics tools, including Domain Annotation (PfamScan), GO Annotation (EggNOG database), and KEGG Pathway Annotation (KEGG online service tools).

Co-immunoprecipitation (Co-IP)

Cells were lysed in cell lysis buffer (89900, Thermo Fisher Scientific) supplemented with a protease and phosphatase inhibitor cocktail (P1260, Solarbio), for 30 min at 4 °C. Following lysis, the samples were centrifuged at 12,000 g for 10 min to separate the soluble components. To prepare the input samples, 30 µl of the protein-containing supernatant were collected and denatured by boiling in 5X SDS loading buffer for 5 min. Next, Protein A/G plus agarose beads (SC-2003, Santa Cruz Biotechnology) were added to each incubation sample on a rotating wheel overnight at 4 °C. The agarose beads were washed three times with NP-40 wash buffer. The coimmunoprecipitated proteins were boiled for 5 min in 1X SDS loading buffer. Input and IP samples were analysed by Western blotting using anti-Myc or anti-HA antibodies.

Statistical analysis

Data are presented as mean ± SEM, and statistical analyses were performed using GraphPad PRISM 9 software. Each experiment included at least three independent samples and was replicated at least three times to ensure reproducibility. Comparisons of variances between two groups were conducted using the unpaired, two-tailed Student's t-test, with statistical significance defined as follows: $*p<0.05$, $**p<0.01$, $***p<0.001$, $****p<0.0001$. No significant differences are denoted as n.s.

Results

Knockout of Cep135 in mice causes male infertility

To elucidate the role of *Cep135* in male reproductive, we generated mice with a specific knockout of *Cep135* in their reproductive system utilizing the CRISPR-Cas9 technology and Cre-loxP system (Fig. 1A). Initially, heterozygous mice were obtained and subsequently crossed with wild-type mice, with the offspring's genotypes being accurately determined through PCR analysis (Fig. 1B). A significant depletion of CEP135 protein levels was observed in the testes of *Cep135* cKO mice compared to those of control mice (Fig. 1C). Notably, given the absence of discernible phenotypic differences between wild-type and heterozygous mice, our subsequent investigations focused exclusively on comparing the control and knockout groups. Cumulatively, these results provide unequivocal evidence for the successful creation of *Cep135* knockout mice.

Cep135 conditional knockout mice attain adulthood with no overt health issues, yet their reproductive prowess is severely compromised. Specifically, upon mating with fertile partners, *Cep135* cKO male mice consistently fail to sire offspring (Fig. 1D), unequivocally establishing their infertile status. This phenomenon implies that the absence of *Cep135* disrupts spermatogenesis, a critical process for male fertility. To elucidate the underlying mechanisms of male sterility, we conducted a thorough examination of the testes of *Cep135* cKO mice. Our analysis revealed that, compared to control mice, the testes of *Cep135* cKO adult mice exhibit a notable reduction in size (Fig. 1E). Importantly, while no statistically significant difference in overall body weight was observed between the two groups (Fig. 1F), the testes weight of *Cep135* cKO mice were found to be significantly decreased (Fig. 1G). Consequently, the calculated testis-to-body weight ratio also exhibited a marked decline (Fig. 1H). In summary, these findings provide compelling evidence that *Cep135* knockout exerts a profound impact on testicular development and maturation in mice. Subsequently, we performed H&E staining on the testis and epididymis of both the control group and *Cep135* cKO mice. The H&E staining revealed that, despite the crucial role of *Cep135*, the testicular architecture of *Cep135* cKO mice was preserved, with a comparable distribution of various germ cell types to that of controls (Fig. 1I). To further delineate the spatial expression pattern of *Cep135* within the germ cells, we employed immunofluorescence staining. Our findings indicated that *Cep135* was robustly expressed in normal spermatocytes, round spermatids, and elongating spermatids, but notably absent in mature spermatozoa residing in the epididymis. This exclusive expression pattern implies that *Cep135* is a potential spermatogenesis-related factor that may be indispensable for male fertility (Fig. S1). Collectively, our results underscore the pivotal role of *Cep135* in male development and highlight its potential significance in the intricate process of spermatogenesis.

Cep135 knockout results in abnormal sperm morphology and OAT phenotype

To delve deeper into the mechanisms underlying male infertility, we isolated sperm from the caudal epididymides of both control and *Cep135* cKO mice. Quantitative

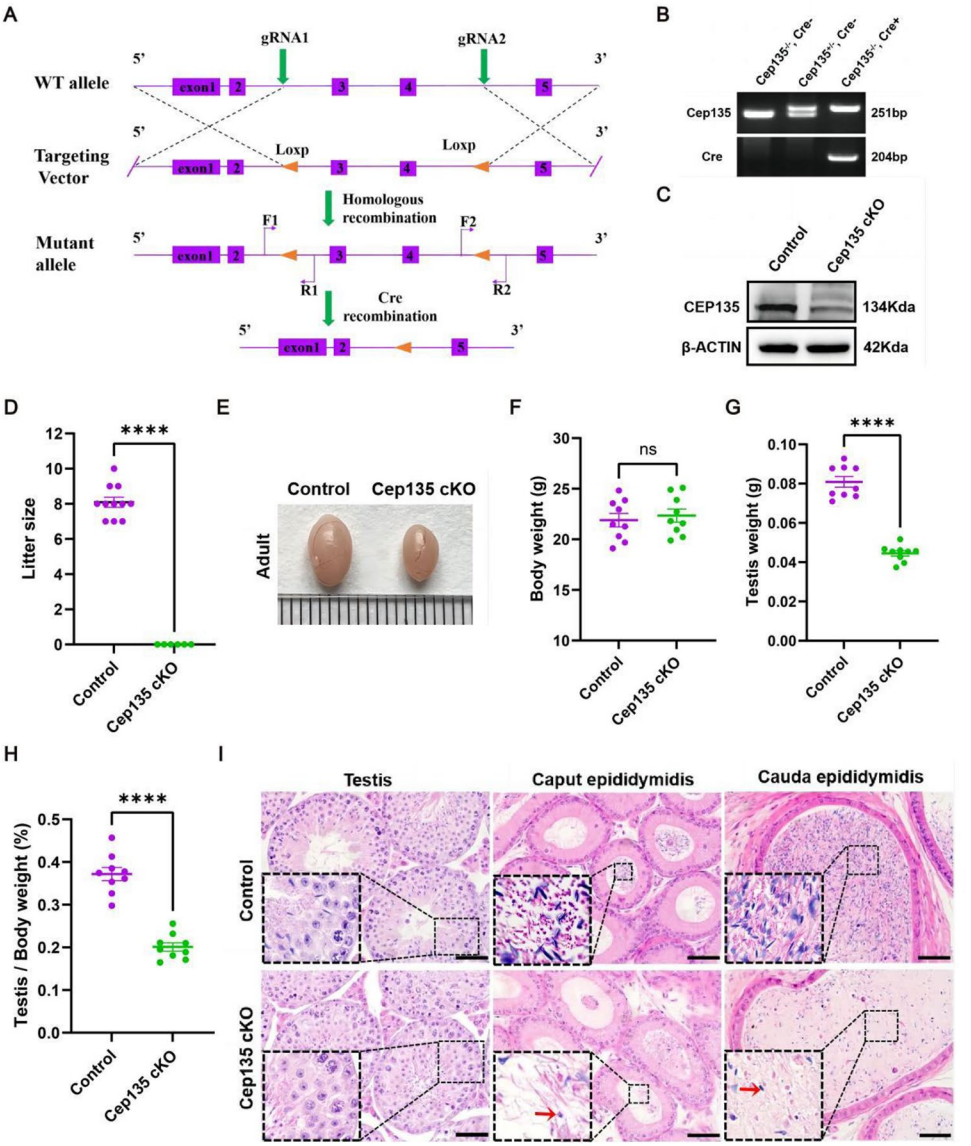

Fig. 1 Disruption of *Cep135* led to male infertility. **(A)** Targeting strategy for the generation of *Cep135* conditional knockout mice. **(B)** Polymerase chain reaction genotyping in control and *Cep135* cKO mice. **(C)** Immunoblotting of CEP135 was performed in testes protein lysates of adult control and *Cep135* cKO mice. β-actin served as a loading control. $n=3$ each group. Representative images were shown. **(D)** Fertility test showing sterile in *Cep135* cKO male mice. $n=11$ for each group. Error bar, mean ± SEM. two-tailed Student's t test; ****$P<0.0001$. **(E)** Determination of testes size in control and *Cep135* cKO mice at 2 months. **(F-G)** Comparison of body weight, testes weight between control and *Cep135* cKO mice at 2 months. $n=9$ for each group. Error bar, mean ± SEM. two-tailed Student's t test; ns, not significant, ****$P<0.0001$. **(H)** Comparison of testes/body weight ratio between control and *Cep135* cKO mice at 2 months. $n=9$ for each group. Error bar, mean ± SEM. two-tailed Student's t test; ***$P<0.001$. **(I)** H&E staining was utilized to observe the structure of the testes and epididymides in control and *Cep135* cKO mice. Scale bar = 50 μm

assessment revealed a substantial reduction in the number of epididymal sperm in *Cep135* cKO mice compared to the control group (Fig. 2A). Further investigation into sperm motility parameters using computer-assisted sperm analysis (CASA) indicated a declining trend in both motile and forward-moving sperm percentages in *Cep135* cKO mice (Fig. 2B-C). Specifically, the curve linear velocity (VCL), straight linear velocity (VSL), and average path velocity (VAP) of epididymal sperm from *Cep135* cKO male mouse (30.54 ± 3.18 μm/s, 13.60 ± 1.54 μm/s, and 27.15 ± 2.84 μm/s, respectively) were significantly lower than those of control (53.71 ± 5.65 μm/s, 25.49 ± 2.98 μm/s, and 48.06 ± 5.08 μm/s, respectively) (Fig. 2D). Histological examination via H&E staining unveiled a variety of morphological abnormalities in *Cep135* cKO sperm, including acrosomal defects, needle-shaped sperm, headless sperm, shorten tail, coiled tail, and ectopia cephalica (Fig. 2E). Statistical analysis of sperm morphology within the epididymides confirmed a significantly higher proportion of sperm with abnormal head and tail morphology in *Cep135* cKO mice compared to controls (Fig. 2F-G), implicating that *Cep135* knockout disrupts spermatogenesis, ultimately resulting in malformed mature sperm. Additionally, immunofluorescence staining of single sperm smears corroborated the H&E staining findings, revealing similar abnormalities in *Cep135* cKO sperm, such as distorted head morphology, acrosomal irregularities, and coiled tails (Fig. S2).

To gain insights into the microstructural alterations, testicular tissue and epididymal sperm from both control and *Cep135* cKO mice were subjected to detailed electron microscopic analysis. TEM of testes samples revealed profound abnormalities in the head morphology of elongated

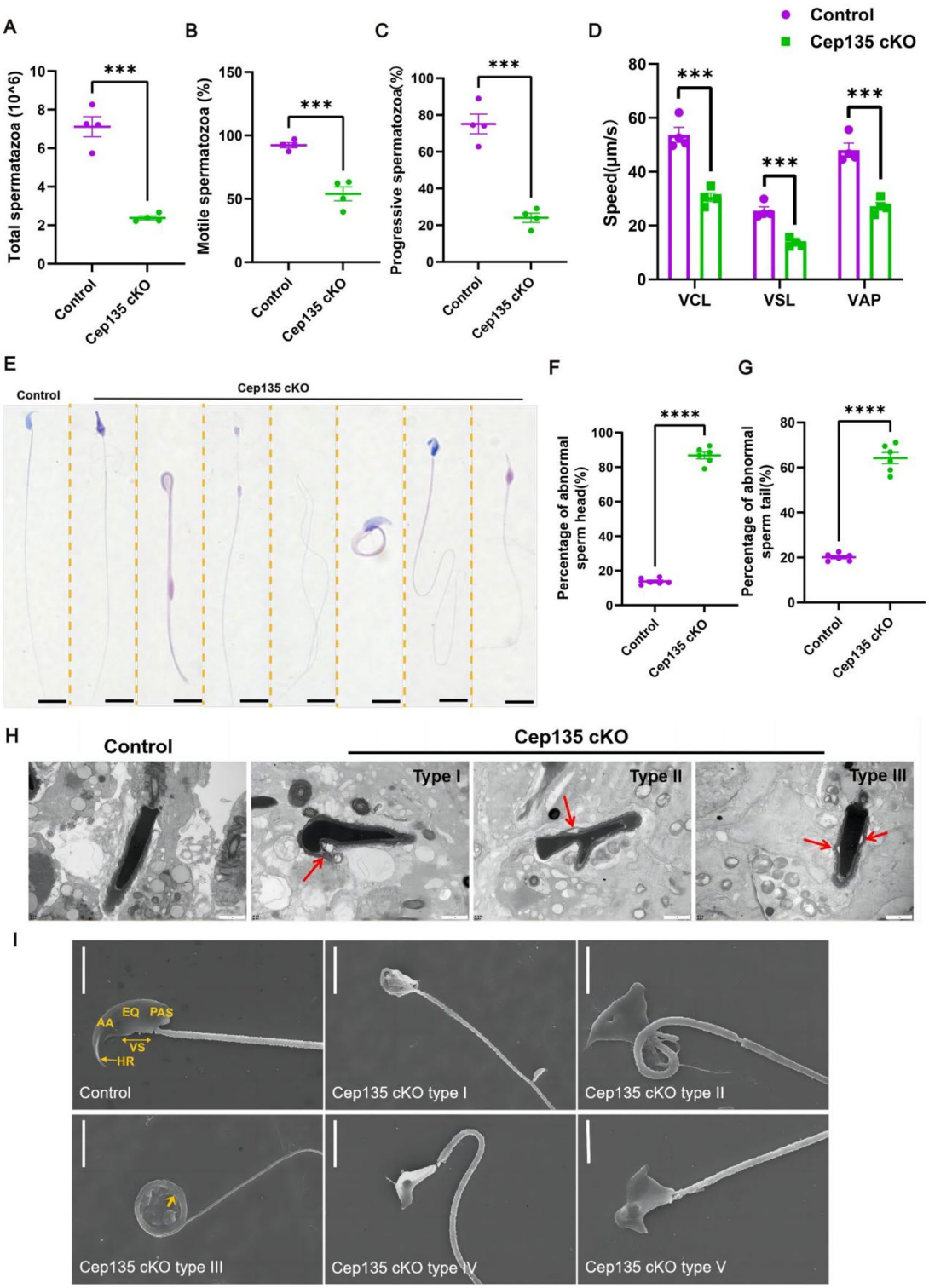
A
Total spermatazoa (10^6)
***
Control
Cep135 cKO
B
Motile spermatozoa (%)
***
Control
Cep135 cKO
C
Progressive spermatozoa(%)
***
Control
Cep135 cKO
D
Control
Cep135 cKO
Speed(μm/s)
***
***
***
VCL
VSL
VAP
E
Control
Cep135 cKO
F
Percentage of abnormal sperm head(%)
****
Control
Cep135 cKO
G
Percentage of abnormal sperm tail(%)
****
Control
Cep135 cKO
H
Control
Cep135 cKO
Type I
Type II
Type III
I
AA
EQ
PAS
VS
HR
Control
Cep135 cKO type I
Cep135 cKO type II
Cep135 cKO type III
Cep135 cKO type IV
Cep135 cKO type V

Fig. 2 *Cep135* cKO mice displayed oligoasthenoteratozoospermia. **(A)** Epididymal sperm number of control and *cep135* cKO mice. $n=4$ for each group. Error bar, mean ± SEM. two-tailed Student's t test; ***$P<0.001$. **(B)** Motile spermatozoa in control and cep135 cKO mice. $n=4$ for each group. Error bar, mean ± SEM. two-tailed Student's t test; ***$P<0.001$. **(C)** Progressive spermatozoa in control and *cep135* cKO mice. $n=4$ for each group. Error bar, mean ± SEM. two-tailed Student's t test; ***$P<0.001$. **(D)** The curve linear velocity (VCL), straight-line velocity (VSL) and average path velocity (VAP) of sperm from control and *Cep135* cKO mice. $n=3$ for each group. Error bar, mean ± SEM. two-tailed Student's t test; ***$P<0.001$. **(E)** H&E staining of the spermatozoa from 2 months control and *Cep135* cKO mice. Spermatozoa from control mice present with typical morphology, while spermatozoa from *Cep135* cKO mice presents an amorphous head accompanied with various head and flagellum defects, such as acrosomal deformed, coiled. Scale bars = 10 μm. **(F)** The percentage of abnormal sperm head morphology observed in control and *Cep135* cKO caudal epididymis. $n=6$ for each group. Error bar, mean ± SEM. two-tailed Student's t test; ****$P<0.0001$. **(G)** The percentage of abnormal sperm tail morphology observed in control and *Cep135* cKO caudal epididymis. $n=6$ for each group. Error bar, mean ± SEM. two-tailed Student's t test; ***$P<0.001$. **(H)** Transmission electron microscopy analysis of the testes in adult control and *Cep135* cKO mice. Germ cells from testis tubules of control mice present with typical morphology, while germ cells from *Cep135* cKO mice presents abnormal head morphology, such as bifurcated (Type II), seperated karyolemma (Type III). Scale bars = 1 μm. **(I)** Scanning electron microscopy analysis of spermatozoa from the epididymis of control and *Cep135* cKO mice. Several abnormal sperm phenotypes were observed: abnormal head shape, curly tail and head absent. Scale bars = 5 μm

sperm in *Cep135* cKO mice. These abnormalities encompassed various types, including curled heads (Type I), bifurcated heads (Type II), and irregular perinuclear membranes (Type III), all of which deviated significantly from the normal elongated sperm head morphology observed in the control group (Fig. 2H). Furthermore, SEM was employed to compare the head structures of epididymal sperm between the two groups. The SEM results underscored the marked deviation in the head morphology of defective sperm from *Cep135* cKO mice, which lacked the characteristic flat crescent shape observed in their control counterparts. Specifically, the defective sperm exhibited anterior acrosomal disorders, absence of a distinct equatorial segment, incomplete posterior acrosomal sheath, reduced ventral curvature, and blunt uncinate margins. Additionally, misoriented axoneme components wrapped around the nucleus, abnormal curling of the sperm flagellum's midpiece, and constriction of the principal piece were also observed (Fig. 2I). Collectively, these findings strongly suggest that *Cep135* knockout results in oligoasthenoteratozoospermia.

The knockout of *Cep135* leads to an increase in apoptosis of testicular germ cells, but do not affect the meiosis of spermatocytes

To unravel the mechanisms contributing to oligoasthenoteratozoospermia and sterility in *Cep135* cKO mice, a comprehensive investigation into spermatogonium proliferation and spermatocyte meiosis was undertaken. We analyzed the expression patterns of various cell markers in adult mice (2 months old). Immunofluorescence staining with proliferating cell nuclear antigen (PCNA) was initially performed to assess cellular proliferation status. Notably, no significant difference in the number of proliferating testicular spermatogonia was observed between *Cep135* cKO mice and their control group (Fig. 3A-B). In addition, TUNEL assays revealed a stark increase in the number of apoptotic cells within the convoluted spermatotubules of *Cep135* cKO mice compared to the control group (Fig. 3C-D). To further validate this finding, immunofluorescence staining targeting apoptosis protein markers (BAX, BAD and CLEAVED CASPASE 3) was conducted, confirming a significant elevation in germ cell apoptosis in *Cep135* cKO mice (Fig. 3E-J). Complementing these findings, protein immunoblotting of testicular tissue extracts from both control and *Cep135* cKO mice demonstrated upregulated expression of BAX, BAD and CLEAVED CASPASE 3 in the knockout group (Fig. 3K-L).

Furthermore, we quantified the counts of germ cells and Sertoli cells utilizing DDX4 and SOX9 markers, respectively. Notably, the number of SOX9-positive Sertoli cells remained within normal range in adult *Cep135* cKO mice, whereas the germ cell count was diminished (Fig. S3A-C). To ascertain whether *Cep135* cKO spermatocytes underwent meiosis correctly, testicular sections from 2-month-old mice were immunostained with SCP3 and γ-H2AX antibodies. Immunofluorescence analysis revealed that the synapsis of SCP3-labeled homologous chromosomes in the testes of *Cep135* cKO mice at 2 months was unaffected, and γ-H2AX-marked germ cells had initiated meiosis, activating programmed DNA double-strand breaks (DSBs). No significant differences were observed between the control and *Cep135* cKO mice in this regard (Fig. S3D-F). In summary, following *Cep135* knockout, there was an elevation in germ cell apoptosis within testicular tubules, yet this did not impede spermatocyte meiosis. Consequently, oligoasthenoteratozoospermia, characterized by a reduced number of mature sperms, is primarily attributed to abnormal alterations occurring during the later stages of spermatogenesis.

Cep135 is essential for mouse spermatogenesis

To elucidate the phenotype of sperm head and flagellum abnormalities resulting from *Cep135* knockout, we used periodic acid-schiff staining reagents to stain the specific period of sperm defects. During spermatogenesis, the spermatogenic epithelium can be broadly categorized into 12 stages and further subdivided into 16 steps based on acrosome and sperm morphological developments. These

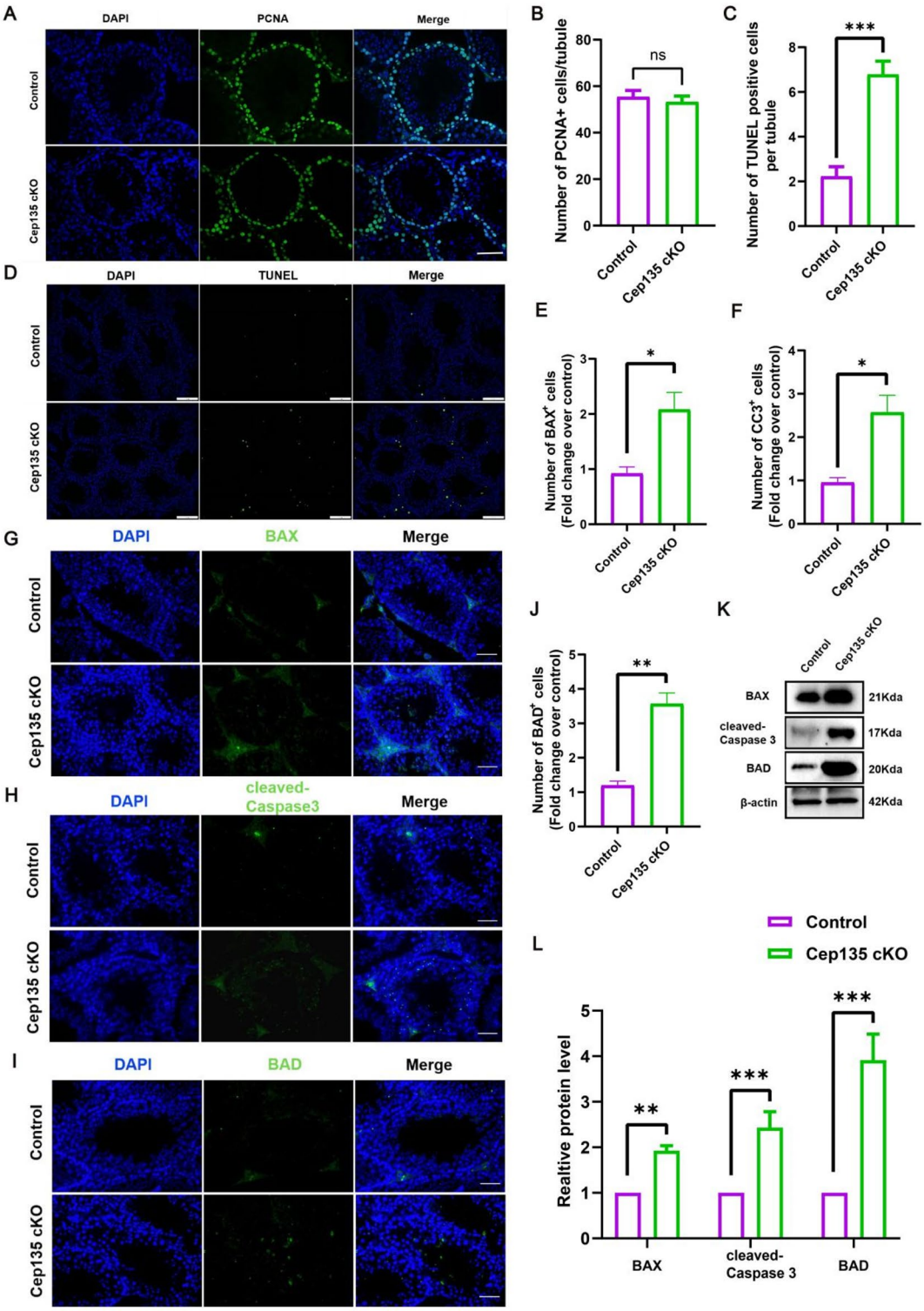
A
DAPI
PCNA
Merge
Control
Cep135 cKO
B
Number of PCNA+ cells/tubule
ns
Control
Cep135 cKO
C
Number of TUNEL positive cells per tubule
***
D
DAPI
TUNEL
Merge
E
Number of BAX+ cells (Fold change over control)
*
F
Number of CC3+ cells (Fold change over control)
*
G
DAPI
BAX
Merge
J
Number of BAD+ cells (Fold change over control)
**
K
Control
Cep135 cKO
BAX
21Kda
cleaved-Caspase 3
17Kda
BAD
20Kda
β-actin
42Kda
H
DAPI
cleaved-Caspase3
Merge
I
DAPI
BAD
Merge
L
Control
Cep135 cKO
Realtive protein level
**
***
***
BAX
cleaved-Caspase 3
BAD

Fig. 3 Abnormal apoptosis in *Cep135* cKO mice testes. **(A-B)** Immunofluorescence staining of PCNA-positive germ cells in control and *Cep135* cKO mice testes at adult. Nuclei were stained with DAPI(blue). Scale bars = 60 μm. Error bar, mean ± SEM. ns, not significant. **(C-D)** Immunofluorescence staining of TUNEL-positive germ cells in control and *Cep135* cKO mice testes at adult. Nuclei were stained with DAPI(blue). Scale bars = 50 μm. Error bar, mean ± SEM. two-tailed Student's t test; ***$P < 0.001$. **(E-G)** Immunofluorescence staining of BAX-positive cells in control and *Cep135* cKO mice testes at adult. Number of BAX-positive cells per tubule in control and *Cep135* cKO mice testes. Nuclei were stained with DAPI(blue). Scale bars = 50 μm. Error bar, mean ± SEM. two-tailed Student's t test; *$P < 0.05$. **(F-H)** Immunofluorescence staining of cleaved-Caspase 3-positive cells in control and *Cep135* cKO male mice at adult. The number of cleaved caspase 3-positive cells per tubule in control and *Cep135* cKO male mice testes. Nuclei were stained with DAPI(blue). Scale bars = 50 μm. Error bar, mean ± SEM. two-tailed Student's t test; *$P < 0.05$. **(I-J)** Immunofluorescence staining of BAD-positive cells in control and *Cep135* cKO male mice at adult. The number of BAD-positive cells per tubule in control and *Cep135* cKO male mice testes. Nuclei were stained with DAPI(blue). Scale bars = 50 μm. Error bar, mean ± SEM. two-tailed Student's t test; **$P < 0.01$. **(K-L)** Western blot was used to detect the protein expression levels of BAX, BAD and cleaved-Caspase 3 in the testes of control and *Cep135* cKO mice. Error bar, mean ± SEM. two-tailed Student's t test; **$P < 0.01$,***$P < 0.001$

transitions, from round to elongated sperm, can be visually observed in testicular sections. In the testicular sections of *Cep135* cKO mice, abnormal and prolonged spermatogenic morphological alterations were discernible during the 10th stage of spermatogenesis (Fig. 4A). To pinpoint the specific period of these defects, we conducted a detailed analysis across the 16 steps of spermatogenesis. At steps 1 through 9, the morphology of the acrosome and sperm nucleus in testicular sections from both *Cep135* cKO mice and control mice remained comparable. However, starting from step 10, abnormal morphological changes in the acrosome and sperm head became evident, ultimately leading to the formation of abnormal sperm at step 16 (Fig. 4B). These findings underscore the pivotal role of *Cep135* in the later stages of spermatogenesis.

Cep135 disruption resulted in the impairment of the acrosome, manchette, and HTCA (head-to-tail connecting apparatus) structures within sperm

We focusing on the manchette structure, which is crucial for shaping the mouse sperm head [14, 56], we observed that the manchette of *Cep135* cKO mice remained normal until the 10th step of spermatogenesis, with abnormal elongation commencing at the 11th step (Fig. 5A). To further examine acrosomal development, we employed TEM detection. Our TEM analysis revealed diverse acrosomal abnormalities in *Cep135* cKO testicular sections, including acrosome disappearance, abnormal sperm head indentation, and nuclear plasma membrane detachment, ultimately contributing to aberrant sperm head morphology (Fig. 5B). Additionally, we performed ultrastructural analysis of sperm flagella from both control and *Cep135* cKO mice using TEM. Notably, the sperm flagella segments of *Cep135* cKO mice exhibited severe disruptions in the (9 + 2) structure, encompassing disturbances in the outer dense fiber (ODF) architecture, microtubule organization, and pronounced absence of surrounding microtubule pairs (Fig. 5C). To investigate the specific stages impacted by *Cep135* knockout, we conducted immunofluorescence analysis using lectin peanut agglutinin (PNA) to label the acrosome and AC-TUBULIN to assess flagellar organization. Our findings revealed that the flagella of *Cep135* cKO spermatids were shorter and disorganized from stages X-XII, in contrast to those of control spermatids (Fig. S4). Additionally, it is established that the sperm flagellum must be anchored to the head by the head-to-tail connecting apparatus (HTCA) to achieve a complete sperm morphology [59, 65]. Thus, we employed TEM to observe the structure of the head-tail junction in testicular sperm. Our TEM results demonstrated that in *Cep135* cKO round spermatids, the basal structure was abnormally distant from the head, with the proximal centriole (PC), segmented column (SC), and capitulum (CP) structures remaining indistinct. Notably, the head-tail junction remained significantly distant even at steps 7–9, with PC, SC, and CP still absent, indicating abnormal flagellar formation. At the elongated spermatids stage, the flagellar structure remained abnormal (Fig. 5D). In conclusion, these results suggest that *Cep135* deletion disrupts the structures of acrosome, manchette and head-tail junction during spermatogenesis.

Aberrant expression of multiple spermatogenesis associated proteins in *Cep135* cKO male mice

Spermatogenesis represents a highly intricate biological process orchestrated by a coordinated network of multiple genes. To delve into how *Cep135* deficiency leads to sperm impairment, we employed proteomics techniques to conduct a comprehensive analysis of testicular lysates from both control and *Cep135* cKO mice. A total of 7254 proteins were quantified in proteomics, with the results visually presented through a volcano plot, revealing 144 proteins upregulated and 235 proteins downregulated (Fig. 6A). Subsequently, we conducted a preliminary screening of these differentially expressed proteins, followed by functional annotation and pathway enrichment analyses. The analysis outcomes indicated that the downregulated proteins in the *Cep135* knockout group were primarily associated with crucial biological processes (BP) or cellular components (CC) such as cilium assembly, axonemal dynein complex assembly, 9 + 2 motile cilium, acrosomal vesicle, sperm fibrous sheath, and outer dense fibers. Conversely, the upregulated proteins were

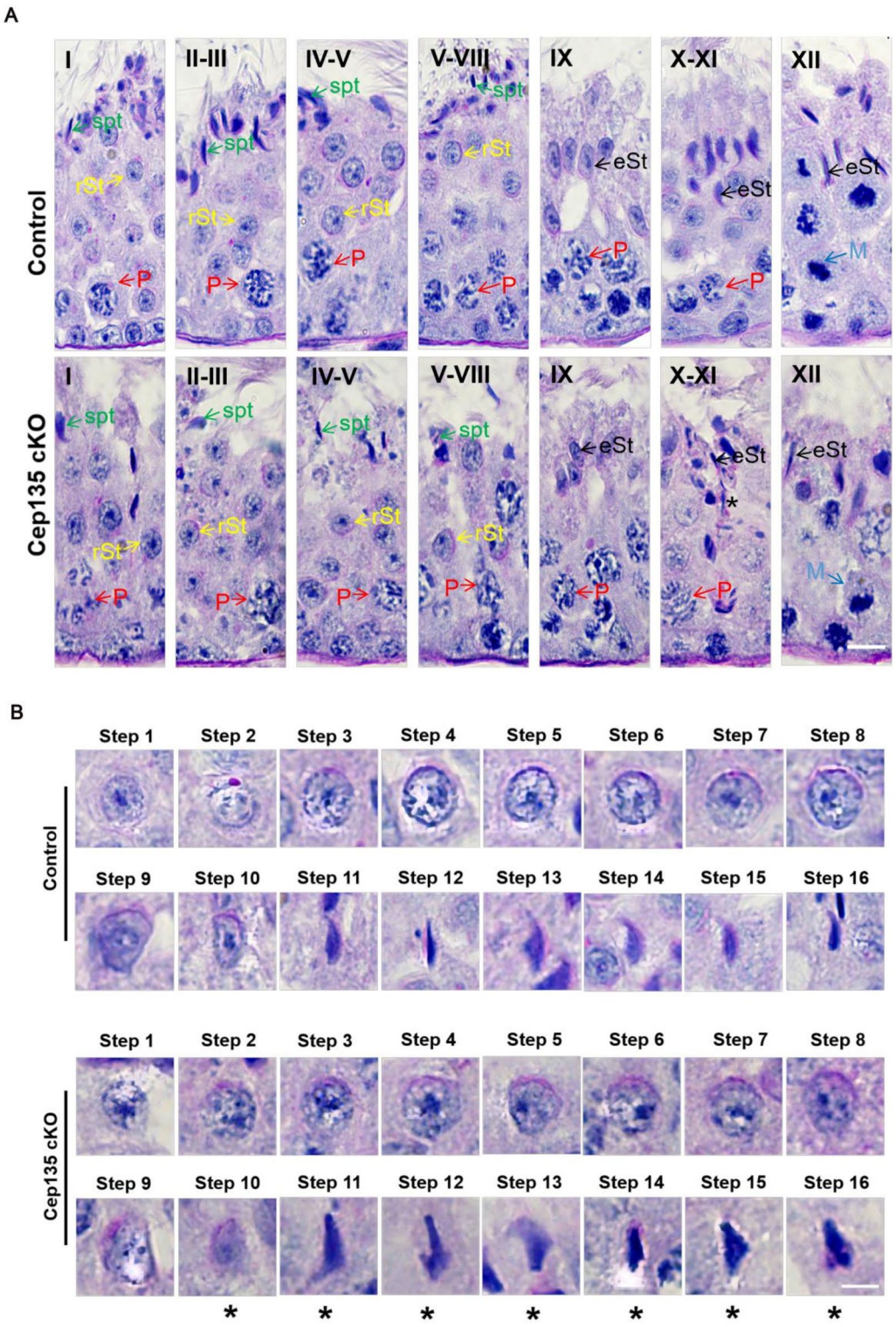

Fig. 4 Spermatogenesis is impaired in *Cep135* cKO mice. **(A)** PAS-hematoxylin staining of *Cep135* cKO testes sections showed abnormal sperm nuclear shape. rSt, round spermatid; spt, spermatozoa; M, meiotic spermatocyte; eSt, elongating spermatid. The asterisk indicates abnormally elongated spermatids at stageX-XI in *Cep135* cKO mice. Scale bar = 10 μm. **(B)** PAS-hematoxylin staining of spermatids at different steps from control and *Cep135* cKO mice. The asterisk indicates abnormally elongated spermatids from step10 to step 16 in *Cep135* cKO mice. Scale bar = 5 μm

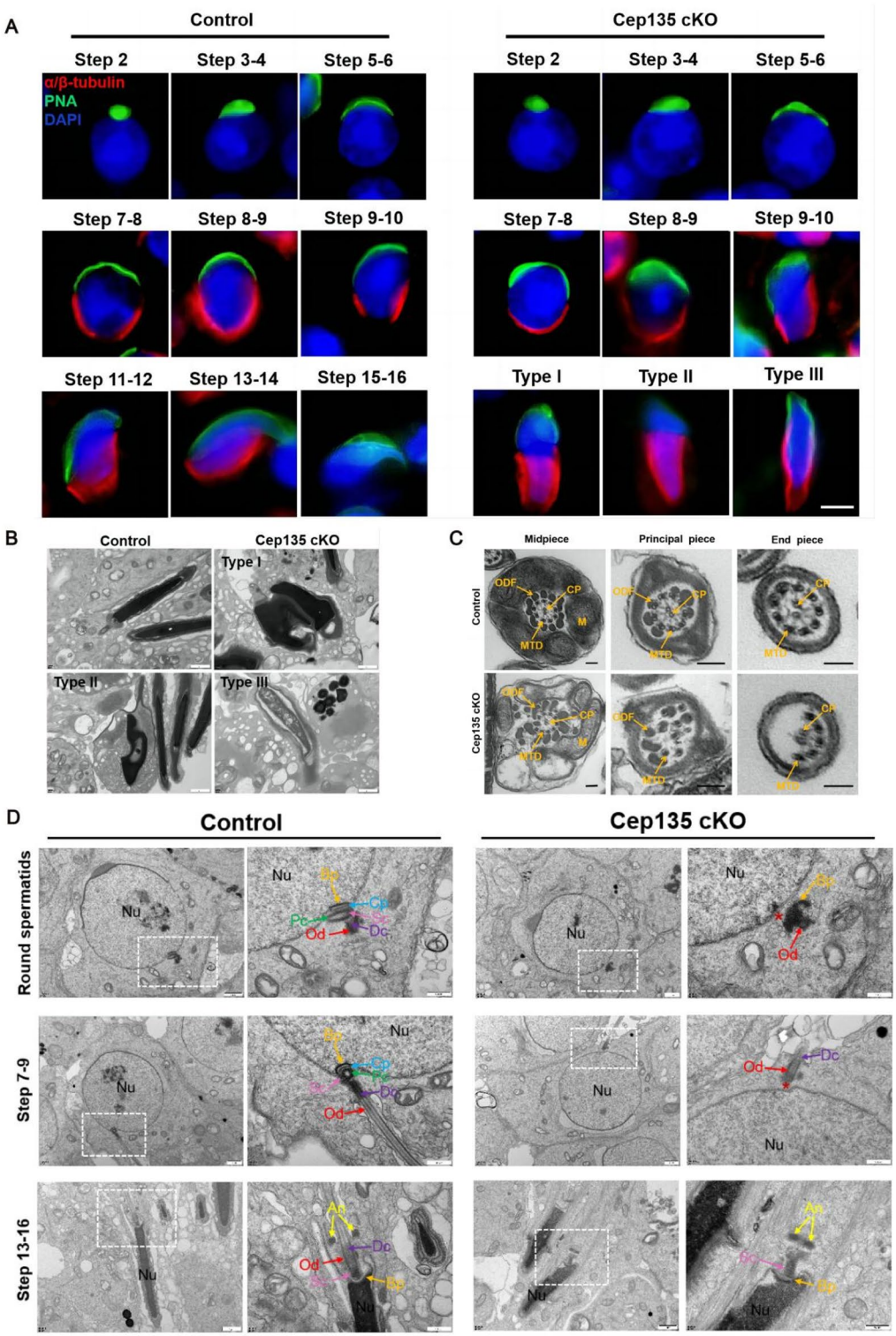
A
Control
Cep135 cKO
Step 2
Step 3-4
Step 5-6
α/β-tubulin
PNA
DAPI
Step 7-8
Step 8-9
Step 9-10
Step 11-12
Step 13-14
Step 15-16
Type I
Type II
Type III
B
Control
Cep135 cKO
Type I
Type II
Type III
C
Midpiece
Principal piece
End piece
Control
Cep135 cKO
ODF
CP
M
MTD
D
Control
Cep135 cKO
Round spermatids
Step 7-9
Step 13-16
Nu
Ac
Bp
Cp
Pc
Sc
Od
Dc

Fig. 5 Disorganized acrosome, manchette and HTCA in *Cep135* cKO mice. **(A)** Abnormal manchette elongation in *Cep135* cKO spermatids. Spermatids from different manchette-containing steps were stained with antibodies against α/β- TUBULIN (red) and LECTIN PNA (green, acrosome marker) to visualize the manchette. *Cep135* cKO spermatids displayed different types of abnormal elongation of the manchette. Nuclei were stained with DAPI (blue). Scale bar = 5 μm. **(B)** The spermatozoa head showed irregular shapes in *Cep135* cKO mice. Scale bar = 1 μm. **(C)** Cross-sections of *Cep135* cKO sperm tails revealed the disorganized or absent axonemal microtubules and tail accessory structures. *Cep135* cKO spermatids displayed outer dense fibers and microtubule disorganized arrange. Scale bar = 100 nm. **(D)** The sperm tail cannot be tightly attached to the sperm head in *Cep135* cKO mice, the different development of spermatogenesis in the testis of cKO in the control group and *Cep135* was analyzed by transmission electron microscopy. The red asterisk indicates the gap between the nuclear membrane and the coupler. Nu: nuclear, Bp (orange): basal plate, Cp (blue): capitulum, Sc (pink): segmented column, Pc (green): proximal centriole, Dc (purple): distal centriole, An (yellow): annulus, Od (red): outer dense fibers. Biologically independent mice were examined in three separate experiments with similar results. Scale bar = 1 μm

intimately linked to endoplasmic reticulum and ribosome functions.

Notably, among the downregulated proteins, 30 were directly involved in spermatogenesis, 25 were related to cilium formation, 19 were intimately connected to acrosomal vesicle function, and an additional 20 were associated with fertilization-related functions. Critically, the reduction in key proteins such as cation channel sperm-associated protein 1 and 4 (CATSPER 1,4), outer dense fiber protein 2 (ODF2), spermatogenesis-associated protein 6 (SPATA6), calcium-binding tyrosine phosphorylation-regulated protein (CABYR), outer dynein arm-docking complex subunit 2 (ODAD2), and testis-specific serine/threonine-protein kinase 2 (TSSK2) likely constitutes a significant contributor to defects in mouse spermatogenesis (Fig. 6B-C). Furthermore, to gain insights into the intricate protein interactions of CEP135, which is pivotal for human and/or mouse reproduction, we utilized the STRING software, specifically focusing on protein-protein interactions (PPIs). This analysis delved into pivotal events during spermatogenesis, encompassing spermatogenesis itself, acrosome-associated proteins, and cilia formation. By connecting multiple significantly differentially expressed predictive proteins in *Cep135* cKO mice, our results underscore the complex interplay among proteins involved in these processes (Fig. 6D). Based on the proteomic analysis outcomes and phenotypic characteristics of *Cep135* cKO mice, we meticulously selected a panel of differentially downregulated proteins intimately associated with sperm flagellar development and acrosome formation for further validation. By collecting testicular protein samples from both control and *Cep135* cKO mice, we conducted western blot experiments, focusing on several proteins including AKAP3 (related to acrosomal vesicles), ODF2 (a crucial component of the microtubule cytoskeleton), SPATA6 (a head-tail linker protein), CABYR and ROPN1 (core proteins involved in sperm flagellum development). The results unequivocally demonstrated a significant downregulation of these proteins in the testicular tissues of *Cep135* cKO mice (Fig. 6E-F). Notably, despite thorough examination, no discernible difference in TSSK4 protein expression was observed in the testicular tissues of *Cep135* cKO mice (Fig. S5). This finding further emphasizes the pivotal role of *Cep135* in spermatogenesis, particularly in acrosome formation, head-tail junction, and flagellar development, and highlights the potential dysfunction of related proteins following *Cep135* knockout. To comprehensively validate this conclusion, we also extracted sperm proteins from both control and *Cep135* cKO mice for Western blot analysis. Consistent with our findings in testicular tissues, the expression of these key proteins in sperm also exhibited a downward trend following *Cep135* knockout (Fig. 6G-H). Additionally, during the cellular component enrichment analysis, we noted a prominent change associated with the plasma membrane. To visually observe this alteration, we performed transmission electron microscopy on the testicular tissues of control and *Cep135* cKO mice. Remarkably, *Cep135* knockout resulted in abnormal separation of the head plasma membrane during spermatogenesis, a phenomenon that aligns well with our previous descriptions (Figs. 5B and 6I), further corroborating the indispensable role of *Cep135* in maintaining normal sperm development.

The disruption of sperm mitochondrial electron transport systems, abnormal elevation of NADPH oxidase activity, or excessive stimulation of amino acid oxidase activity are all recognized as potential key factors contributing to oxidative stress [2]. In our proteomic analysis, we prominently observed numerous proteins involved in the regulation of NADPH oxidoreductase activity. Consequently, we utilized immunofluorescence and western blot techniques to examine the expression levels of oxidative stress markers, 3-nitrotyrosine (3-NT) and 4-hydroxynonenal (4-HNE), in the testes of adult mice. The results indicated that the expressions of both markers were significantly upregulated in the germ cells of *Cep135* cKO mice compared to the control group. This finding suggests that the absence of *Cep135* leads to an increase in reactive oxygen species (ROS) levels, which may subsequently induce apoptosis and damage in the cells. Given that mitochondria are the primary sites of ROS generation within cells and are crucial for maintaining redox homeostasis [43], we further explored the impact of *Cep135* cKO on mitochondrial expression in mouse testes, then assessed the expression of Tom20, a marker of the mitochondrial outer membrane, in the testes of adult mice. Surprisingly, the results showed no significant difference in mitochondrial abundance between the control and *Cep135*

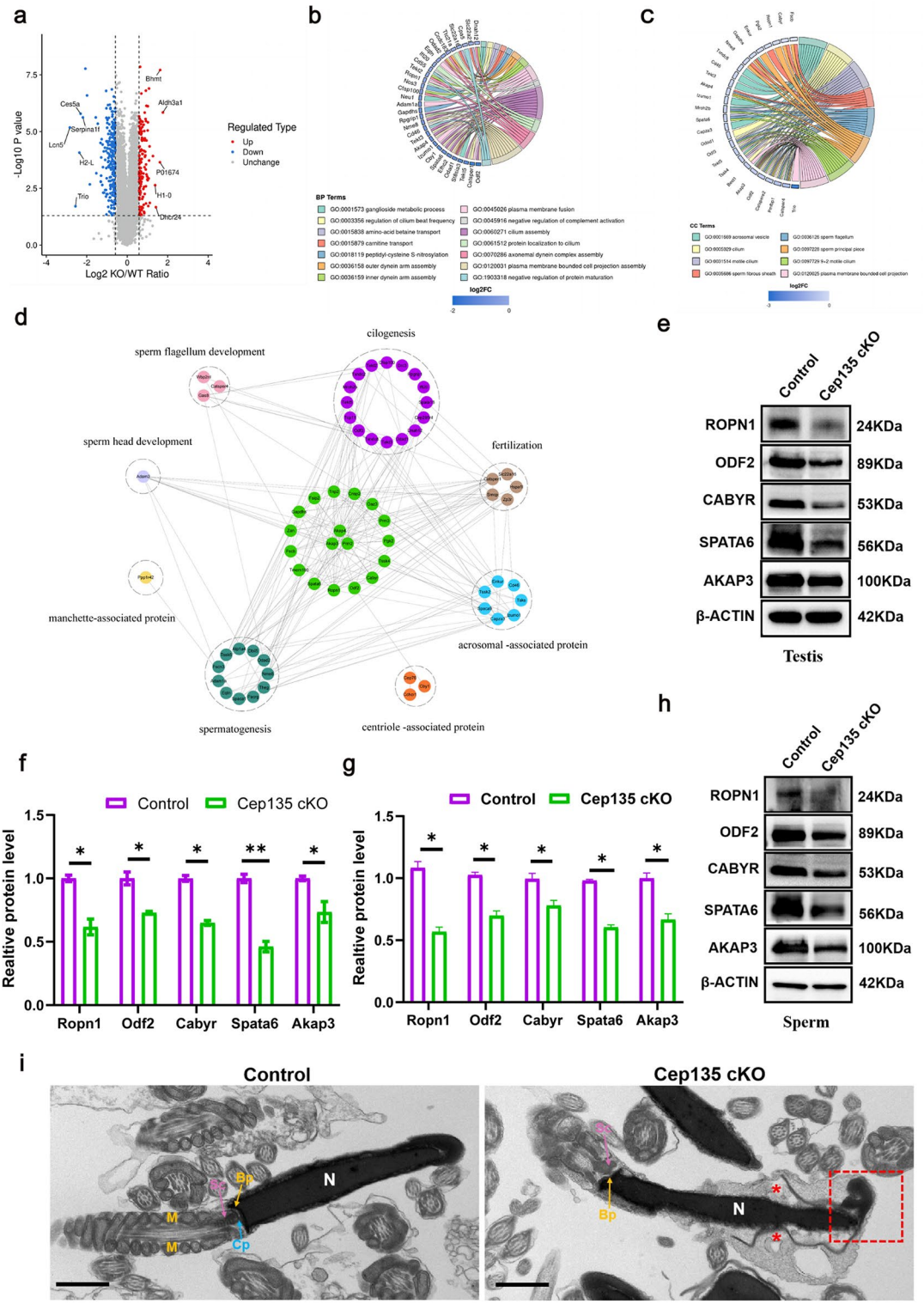
a
-Log10 P value
Log2 KO/WT Ratio
Regulated Type
Up
Down
Unchange
Bhmt
Aldh3a1
Ces5a
Serpina1f
Lcn5
H2-L
P01674
H1-0
Trio
Dhcr24
b
BP Terms
GO:0001573 ganglioside metabolic process
GO:0003356 regulation of cilium beat frequency
GO:0015838 amino-acid betaine transport
GO:0015879 carnitine transport
GO:0018119 peptidyl-cysteine S-nitrosylation
GO:0036158 outer dynein arm assembly
GO:0036159 inner dynein arm assembly
GO:0045026 plasma membrane fusion
GO:0045916 negative regulation of complement activation
GO:0060271 cilium assembly
GO:0061512 protein localization to cilium
GO:0070286 axonemal dynein complex assembly
GO:0120031 plasma membrane bounded cell projection assembly
GO:1903318 negative regulation of protein maturation
log2FC
c
CC Terms
GO:0001669 acrosomal vesicle
GO:0005929 cilium
GO:0031514 motile cilium
GO:0036126 sperm flagellum
GO:0097228 sperm principal piece
GO:0097729 9+2 motile cilium
GO:0120025 plasma membrane bounded cell projection
log2FC
d
cilogenesis
sperm flagellum development
sperm head development
fertilization
manchette-associated protein
acrosomal -associated protein
spermatogenesis
centriole -associated protein
e
Control
Cep135 cKO
ROPN1
ODF2
CABYR
SPATA6
AKAP3
β-ACTIN
24KDa
89KDa
53KDa
56KDa
100KDa
42KDa
Testis
f
Control
Cep135 cKO
Realtive protein level
Ropn1
Odf2
Cabyr
Spata6
Akap3
g
Control
Cep135 cKO
Realtive protein level
Ropn1
Odf2
Cabyr
Spata6
Akap3
h
Control
Cep135 cKO
ROPN1
ODF2
CABYR
SPATA6
AKAP3
β-ACTIN
24KDa
89KDa
53KDa
56KDa
100KDa
42KDa
Sperm
i
Control
Cep135 cKO
N
Bp
Cp
M
M
N
Bp

Fig. 6 Proteomics analysis of differentially expressed protein in *Cep135* cKO mice. (**A**) Volcano plot depicting the protein differences between control and *Cep135* cKO testes. Proteins that exhibited a > 2 fold change in abundance and had a P value < 0.05 are shown in red (up regulated) or blue (down regulated). (**B**) GO terms enrichment analysis of downregulated differential proteins. (**C**) CC terms enrichment analysis of downregulated differential proteins. (**D**) The interaction network of CEP135 with other proteins from different functional groups analyzed using the STRING software. Centering on CEP135 interacting proteins, the network maps protein interactions associated with multiple functional classes, all of which are significantly different in omics. (**E-F**) Western blotting (WB) validated the expression of ROPN1, ODF2, CABYR, SPATA6, AKAP3 in testes from control and *Cep135* cKO mice. β-actin served as a loading control. $n = 3$ for each group. Error bar, mean ± SEM. two-tailed Student's t test; $^{*}P < 0.05$, $^{**}P < 0.01$. (**G-H**) Relative protein levels of CEP135 and ROPN1, ODF2, CABYR, SPATA6, AKAP3 in spermatids of Cep135 cKO mice and their littermate control mice. β-actin served as a loading control. $n = 3$ for each group. Error bar, mean ± SEM. two-tailed Student's t test; $^{*}P < 0.05$. (**I**) The morphology of spermatogenesis in the testis of control group and Cep135 cKO was analyzed by transmission electron microscopy. N: nuclear, Bp (orange): basal plate, Cp (blue): capitulum, Sc (pink): segmented column, M (green): mitochondrion. Scale bar = 1 μm

cKO groups (Fig. S6A-H). In summary, these findings reveal that the deletion of *Cep135* contributes to spermogenesis abnormalities through its effects on the expression of proteins intimately related to sperm acrosome formation, flagellar development, and head-tail connection, as well as by exacerbating oxidative stress responses.

CEP135 interacts with SPATA6 and regulates sperm head-to-tail junction and ciliogenesis

Based on our initial protein screening, we uncovered the pivotal roles of SPATA6 and AKAP3 proteins in sperm head-tail connection, flagellar structure, and male reproductive function. It indicated that the absence of these proteins directly leads to male infertility [29, 35, 61, 63]. Further investigations at the protein level revealed that the knockout of CEP135 significantly decreased the expression levels of SPATA6 and AKAP3. Consequently, we formulated a hypothesis: CEP135 might play a crucial role in regulating mouse spermatogenesis through its interaction with SPATA6 and/or AKAP3. To validate this hypothesis, we first utilized co-immunoprecipitation (co-IP) and western blot analysis in HEK293T cells overexpressing tagged proteins. These experiments successfully confirmed the direct protein-protein interactions between CEP135 and both SPATA6 and AKAP3, providing robust support for our hypothesis (Fig. 7A-D).

Subsequently, we delved deeper into cellular validation and confirmed the efficacy of *Cep135* knockdown and observed a significant decrease in SPATA6 protein levels in NIH3T3 cells transfected with *Cep135* siRNA compared to those transfected with scramble siRNA. Notably, this decrease could be partially rescued by expressing an exogenous Cep135-HA with synonymous mutations in the siRNA-binding region, while the interference effect on AKAP3 was present but less pronounced (Fig. 7E-H).

To investigate whether CEP135 regulates its partner protein SPATA6 by affecting protein stability, we treated HEK293T cells overexpressing SPATA6 and CEP135 or lacking CEP135 with cycloheximide (CHX) for 12 h to block protein synthesis. Experimental results demonstrated that the presence of CEP135 significantly slowed down the degradation rate of SPATA6 (Fig. 7I-K), indicating that CEP135 plays a pivotal role in maintaining the stability of SPATA6. Moreover, proteomic analysis revealed that many of the downregulated proteins in the *Cep135* knockout group were associated with cilium assembly. To further elucidate the regulatory role of *Cep135* in cilium formation, we knocked down endogenous *Cep135* using siRNA and measured cilium length in NIH3T3 cells under cilium-inducing conditions. Our results showed that compared to the control group, *Cep135* knockdown significantly reduced cilium length, and this effect could be reversed by introducing an Cep135-HA synonymous mutation in the siRNA-binding region (Fig. 7L, M). This underscores the critical importance of Cep135 in the normal formation of cilia. In summary, Cep135 may directly or indirectly regulate sperm head-tail connection, flagellar biogenesis, and even cilium assembly processes through its interaction with proteins such as SPATA6, thereby contributing to the infertility phenotype observed in *Cep135* deficient mice. This discovery not only enhances our understanding of the mechanisms underlying male reproductive development but also presents novel potential targets for the treatment of related infertility disorders.

Discussion

Cep plays an irreplaceable and vital role in the biogenesis of centrioles and the intricate regulation of the cell cycle. Previous studies have implicated homozygous mutations in *Cep135*, identified through whole-exome sequencing, as being associated with human MMAF, ultimately leading to male infertility. However, the specific underlying mechanisms of *Cep135* in spermatogenesis and male infertility remain elusive. Drawing upon preliminary clinical reports, we have generated the conditional *Cep135* knockout mouse model using *Stra8*-Cre, directly demonstrating that the functional loss of *Cep135* is a pivotal factor underlying male infertility. Furthermore, we speculate that CEP135, through its interaction with SPATA6, plays a critical role in regulating sperm head-to-tail connection and flagellar biogenesis, thereby profoundly influencing the overall process

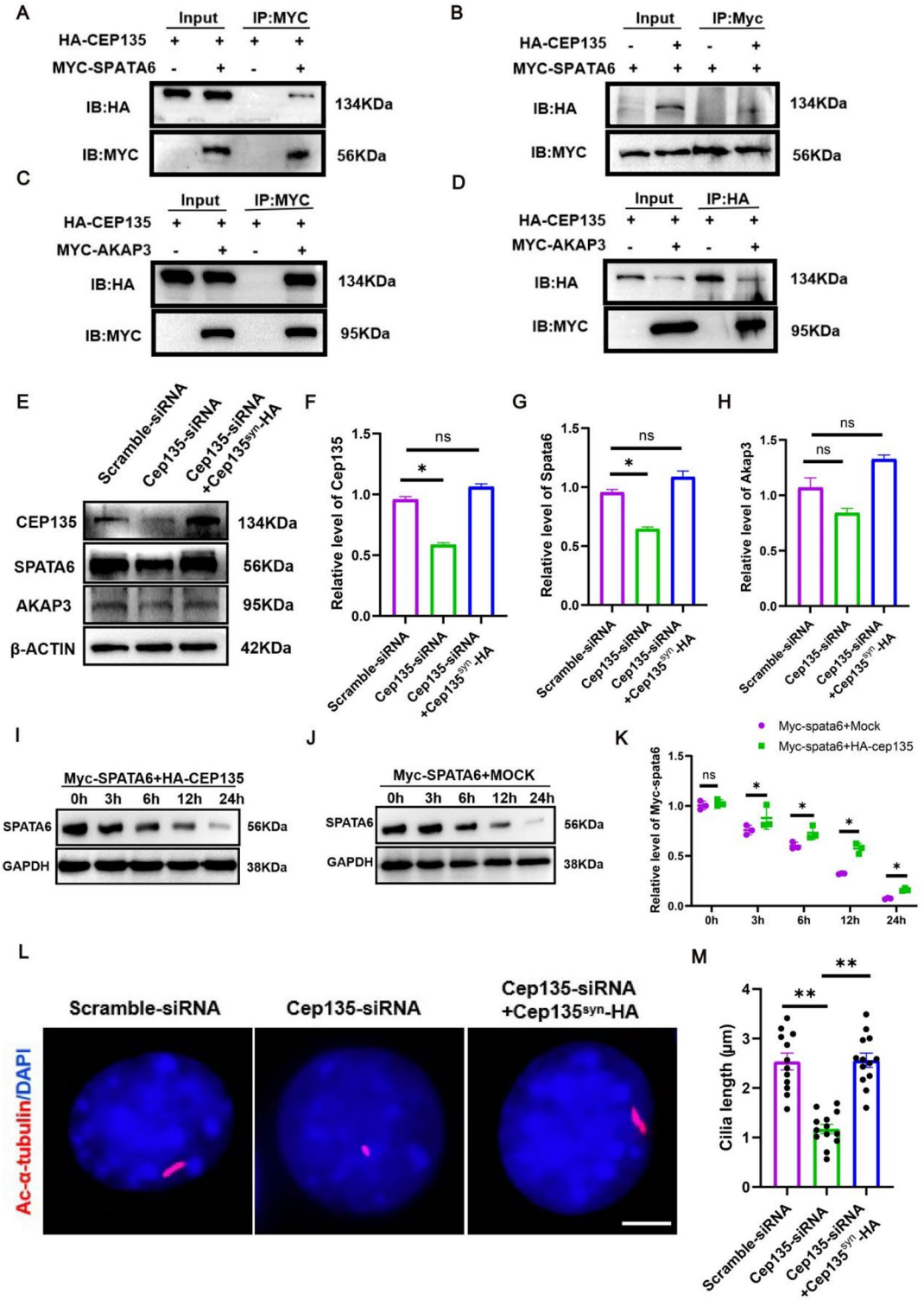
A
Input
IP:MYC
HA-CEP135 + + + +
MYC-SPATA6 - + - +
IB:HA
IB:MYC
134KDa
56KDa
B
Input
IP:Myc
HA-CEP135 - + - +
MYC-SPATA6 + + + +
IB:HA
IB:MYC
134KDa
56KDa
C
Input
IP:MYC
HA-CEP135 + + + +
MYC-AKAP3 - + - +
IB:HA
IB:MYC
134KDa
95KDa
D
Input
IP:HA
HA-CEP135 + + + +
MYC-AKAP3 - + - +
IB:HA
IB:MYC
134KDa
95KDa
E
Scramble-siRNA
Cep135-siRNA
Cep135-siRNA +Cep135syn-HA
CEP135
SPATA6
AKAP3
β-ACTIN
134KDa
56KDa
95KDa
42KDa
F
Relative level of Cep135
ns
*
Scramble-siRNA
Cep135-siRNA
Cep135-siRNA +Cep135syn-HA
G
Relative level of Spata6
ns
*
H
Relative level of Akap3
ns
ns
I
Myc-SPATA6+HA-CEP135
0h 3h 6h 12h 24h
SPATA6
GAPDH
56KDa
38KDa
J
Myc-SPATA6+MOCK
0h 3h 6h 12h 24h
SPATA6
GAPDH
56KDa
38KDa
K
Myc-spata6+Mock
Myc-spata6+HA-cep135
Relative level of Myc-spata6
ns
*
0h 3h 6h 12h 24h
L
Scramble-siRNA
Cep135-siRNA
Cep135-siRNA +Cep135syn-HA
Ac-α-tubulin/DAPI
M
Cilia length (μm)
**
**
Scramble-siRNA
Cep135-siRNA
Cep135-siRNA +Cep135syn-HA

Fig. 7 CEP135 interacts with SPATA6 and regulates its expression. **(A-B)** Coimmunoprecipitation (co-IP) assay indicated that Myc-tagged SPATA6 interacted with HA-tagged CEP135 in HEK293T cells. The co-IP experiments were repeated for three times and representative blots were shown. **(C-D)** Coimmunoprecipitation (co-IP) assay indicated that Myc-tagged AKAP3 interacted with HA-tagged CEP135 in HEK293T cells. The co-IP experiments were repeated for three times and representative blots were shown. **(E-H)** After transfecting NIH3T3 cells with Scramble-siRNA, *Cep135*-siRNA, and *Cep135*-siRNA+Cep135-HA, the expression levels of CEP135, SPATA6 and AKAP3 were verified using WB. β-actin served as a loading control. $n=3$ for each group. Error bar, mean±SEM. two-tailed Student's t test; ns, not significant, $*P<0.05$. **(I-K)** Degradation of MYC-labeled SPATA6 and CEP135 with or without HA labeling in HEK293T cells. After 100 μg/ml of CHX blocked the synthesis of the new protein, the protein sample was harvested at the specified time. β-actin as a load control. The Western blotting experiment was repeated three times with similar results. $n=3$ for each group. Error bar, mean±SEM. two-tailed Student's t test; ns, not significant; $*P<0.05$. **(L-M)** Immunofluorescence analysis (**L**) and length statistics (**M**) of primary cilia in NIH3T3 cells treated by *Cep135* siRNA with or without Cep135-HA synonymous mutation overexpression after serum starvation. AC-TUBULIN (red) and DAPI (blue) were used to stain cilia and nuclei, respectively. $n=11$ for scramble-siRNA group, $n=13$ for *Cep135*-siRNA group, $n=13$ for *Cep135*-siRNA+Cep135-HA group. Scale bar = 5 μm. Error bar, mean±SEM. two-tailed Student's t test; $**P<0.01$

of spermatogenesis (Fig. 8). Thus, our work not only establishes the central position of *Cep135* in mouse spermatogenesis but also uncovers its potential as a novel regulatory mechanism in male infertility.

Members of the CEP family are essential molecules in sperm biology, crucial for the formation of sperm flagella, acrosome development, and the manchette, a transient cytoskeleton structure unique to sperm. Mutations in these genes have been shown to cause reproductive disorders such as oligoasthenospermia and teratozoospermia in both human and mouse models. For instance, knockout of *Cep63*, *Cep70*, *Cep128*, *Cep78* and *Cep131* leads to infertility due to defects in sperm flagella and abnormal development of the acrosome and manchette. In our study, *Cep135* cKO mice exhibited oligoasthenoteratozoospermia and infertility. This divergence may stem from the difference in *Cep135* mutation types reported by Sha et al. compared to our knockout model [49], further emphasizing the complexity and diversity of *Cep135* gene variations in reproductive health.

To delve deeper into the pivotal role of *Cep135* in the male reproductive system, we generated Cep135 cKO mice. Our experimental results demonstrated that these *Cep135*-deficient male mice were completely infertile, accompanied by a marked reduction in testicular weight and a drastic depletion of mature sperm within the epididymis (Figs. 1E and 2A). Further histological analysis unequivocally revealed that the absence of *Cep135* severely impeded the normal progression of spermatogenesis (Fig. 1I). Fertility tests unequivocally confirmed this finding, establishing that *Cep135* knockout directly leads to male infertility in mice (Fig. 1D). Notably, this represents the first scientific report of *Cep135*'s involvement in the regulation of spermatogenesis. Utilizing PAS staining, we observed that upon *Cep135* dysfunction, sperm development encountered a barrier at stage X, specifically manifesting as the failure of round spermatids to undergo normal elongation into elongated spermatids, resulting in the production of morphologically abnormal sperm (Fig. 4A). Spermatozoa analysis revealed a significant decrease in sperm concentration and the number of motile sperm in the epididymis of *Cep135* cKO mice (Fig. 2A-B), a finding that aligns closely with the characteristics of OAT, potentially stemming from excessive apoptosis of germ cells or impaired release of sperm from the seminiferous epithelium. TUNEL assays further corroborated the presence of significant apoptosis among the germ cells of *Cep135* cKO mice (Fig. 2C-D). Of particular interest, in-depth analysis using TEM and SEM unveiled abnormalities in the acrosome and flagellum structures of the testes and sperm of *Cep135* cKO mice, directly contributing to a comprehensive decline in sperm progressive motility, evidenced by marked impairments in mean curvilinear velocity, straight-line velocity, and path velocity (Fig. 2H-I).

Drawing upon previous research, the homologous gene BLD10/CEP135 in *Drosophila* serves as a crucial player in centriole and flagellum biogenesis, capable of binding and stabilizing microtubules and being essential for the early steps of central microtubule pair formation [10]. Integrating our phenotypic analysis, the loss of *Cep135* undeniably leads to the emergence of a typical OAT phenotype (oligozoospermia, asthenozoospermia, and teratozoospermia) in male mice, a symptom cluster commonly observed in infertile men and encompassing various manifestations such as oligozoospermia, asthenozoospermia, and teratozoospermia [44, 55]. Notably, ZP3R (also known as SP56), which localizes to the sperm surface post-capacitation and is released during acrosomal membrane and plasma membrane fusion, may directly impact fertilization processes due to its reduced expression [6]. Additionally, the significant downregulation of IZUMO1 and SPACA1, two membrane proteins crucial for head formation and oocyte fusion, in the testes of *Cep135* cKO mice [9, 62], underscores the pivotal role of CEP135 in the regulation of acrosome formation [52].

Furthermore, through an in-depth analysis of GO annotations, we have identified 61 proteins in *Cep135* cKO mice that are intimately associated with sperm tail development, exhibiting marked downregulation of their expression levels. Notably, previous literature has highlighted that the absence of genes such as *Spata6*, *Ropn1*, and *Cabyr* in mouse models directly leads to structural abnormalities and malformation of the sperm tail [50]. Further investigations reveal that in cases of asthenoteratozoospermia, the

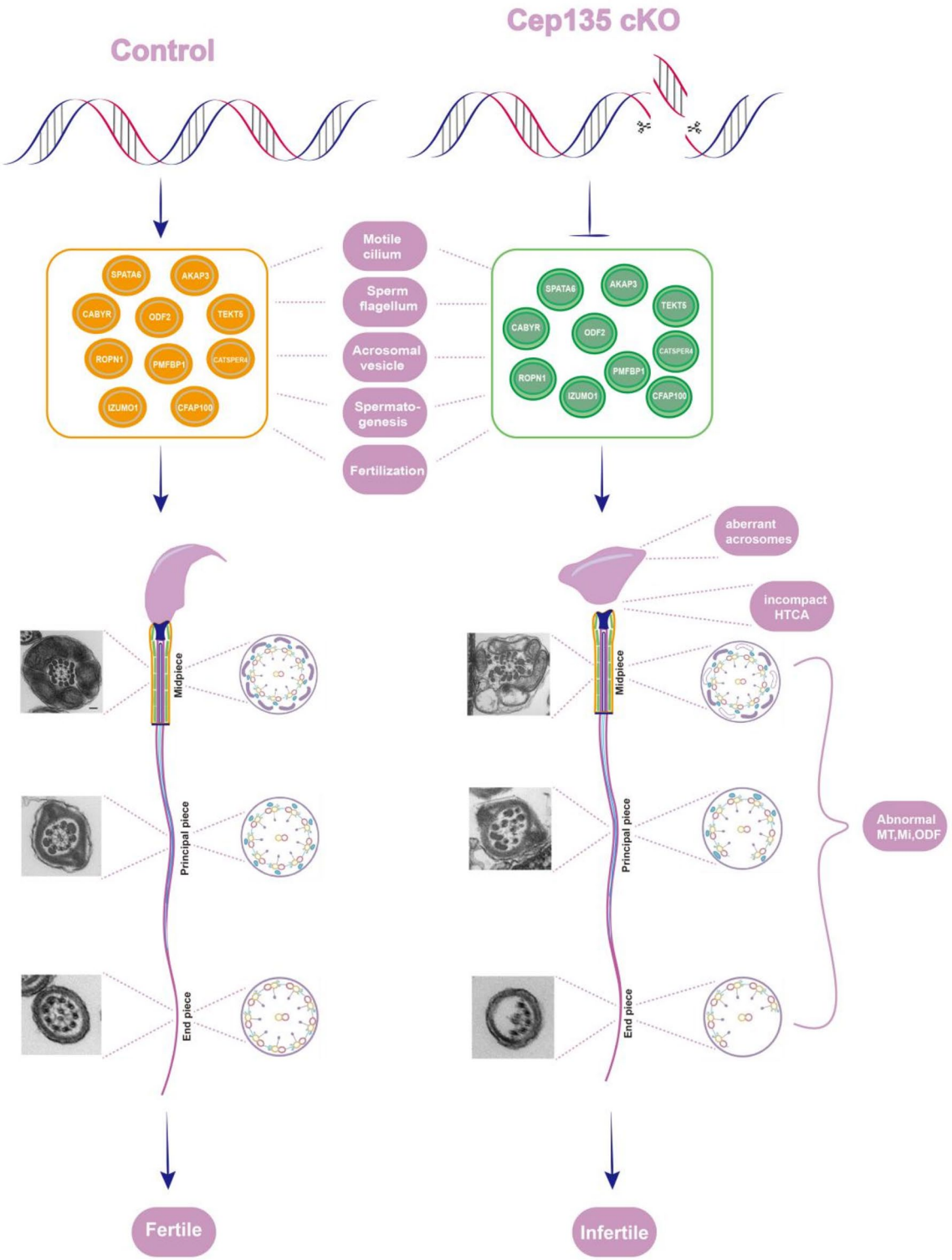

Fig. 8 Schematic Depiction of the Pathogenesis Elicited by CEP135 Deficiency. The absence of CEP135 disrupts the regulated expression and intricate interplay between SPATA6 and AKAP3, two proteins that engage in physical associations with CEP135. This deregulation leads to a cascade of morphological abnormalities, including an elongated manchette, malformed acrosomes, disrupted 9+2 microtubule axonemal organization (MT), absence of mitochondria (Mi) and ODF, weakened head-to-tail coupling apparatus (HTCA), and a curled flagellum

expression levels of ROPN1 and CABYR are significantly reduced. These proteins, by interacting with AKAP3, regulate the PKA signaling pathway, thereby crucially impacting the formation of sperm flagella [34]. Additionally, the lack of spermatogenesis-associated protein 6 (SPATA6) disrupts the normal development of sperm connecting piece and head-tail attachment [63]. Concurrently, testicular-specific serine/threonine protein kinases 1, 2, and 4 (TSSK1, TSSK2, TSSK4) play pivotal roles in sperm flagellar development [47, 57]. Our proteomic data analysis demonstrates that upon CEP135 deletion, the expression of ROPN1, CABYR, SPATA6, TSSK1, TSSK2, TSSK4, and AKAP3 is significantly reduced, directly contributing to the failure of sperm flagellar formation in *Cep135* cKO mice. It is noteworthy that mutations in CAPZA3 have been confirmed to cause male infertility accompanied by an OAT-like phenotype [19], further suggesting that CEP135 deficiency may be another crucial factor triggering OAT phenotypes.

In-depth exploration of CEP135's interacting proteins has revealed direct interactions between CEP135 and key proteins involved in sperm head-tail junction and flagellar formation, namely SPATA6 and AKAP3. The absence of CEP135 leads to downregulation of these two proteins, particularly SPATA6, thereby disrupting their structural stability and adversely affecting the normal development of sperm flagella, resulting in shortened and morphologically abnormal flagella. As a crucial member of the Spata family, SPATA6 is essential for the development of the connecting piece, annulus, and the assembly and maintenance of the flagellum [29, 61, 63]. The assembly of the annulus and flagellum is precisely orchestrated by proximal and distal centrioles, respectively, and the absence of *Cep135* likely disrupts this process, triggering a cascade of pathological changes.

Conclusions

In conclusion, based on genetic and functional data from mouse models, we strongly contend that *Cep135* is a significant causal gene for OAT and male infertility. The loss of *Cep135* not only leads to acrosomal malformation, sperm flagellar defects, but also impairs the normal conjunction of sperm head-to-tail. This study also preliminarily elucidates the potential mechanisms underlying CEP135's regulation of sperm flagellar development and confirms the crucial role of CEP135's interactions with SPATA6 and AKAP3 in maintaining sperm structural stability. Notably, the interaction between CEP135 and SPATA6 is also significant for the regulation of cilia length. Consequently, screening for deleterious mutations in CEP135 holds significant potential value for clinical molecular diagnosis of male infertility. Given the novelty of CEP135 research, further exploration of this gene's central role in male fertility is warranted. This endeavor aims to enrich and fortify the foundation for therapeutic and preventive strategies against human male infertility.

Supplementary Information The online version contains supplementary material available at https://doi.org/10.1007/s00018-025-05616-w.

Author contributions Hui Liu, Zongzhuang Wen, Min Liu and Jiangang Gao Conceived the work, Hui Liu, Zongzhuang Wen and Min Liu designed the experiments, performed data analysis, Haozheng Zhang performed the CO-IP experiments, Tingting Song and Xin Liu performed the cell experiments, Hui Liu, Haozheng Zhang, Guanghao Qin, Tingting Song, Xianmei Wang and Xin Liu performed the WB and immunofluroscence staining experiments. Hui Liu, Xianmei Wang, Xiaolong Fu and Jiangang Gao wrote and revised the manuscript. Min Liu, Xiaolong Fu and Jiangang Gao provided funding support. All authors read and approved the submission.

Funding This work was supported by grants from Medicine Health Science and Technology Development Program of Shandong Province (202201010631, 202205030999), National Natural Science Foundation of China (82401875), Youth Science Foundation Program of Shandong First Medical University(202201-010), Tai an Science and Technology Innovation Development Project (2021NS156), Natural Science Foundation for Youth of Shandong Province (ZR2023QH164, ZR2022QC184).

Data availability The datasets used and/or analysed during the current study are available from the corresponding author on reasonable request.

Declarations

Ethical approval All experimental protocols involving animals were granted approval by the Ethics Committee of Shandong First Medical University (Approval Number: W202211250348, Jinan, China), ensuring strict adherence to Chinese animal protection laws and regulations.

Consent for publication Not applicable.

Conflict of interest The authors have declared that no competing interest exists.

References

1. Agarwal A, Baskaran S, Parekh N et al (2021) Male infertility. Lancet 397:319–333. https://doi.org/10.1016/S0140-6736(20)32667-2
2. Aitken RJ, Drevet JR, Moazamian A et al (2022) Male infertility and oxidative stress: a focus on the underlying mechanisms. Antioxid (Basel) 11. https://doi.org/10.3390/antiox11020306
3. Ameratunga D, Gebeh A, Amoako A (2023) Obesity and male infertility. Best Pract Res Clin Obstet Gynaecol 90:102393. https://doi.org/10.1016/j.bpobgyn.2023.102393
4. Anonymous (2024) Focusing on male infertility. Nat Rev Urol 21:61. https://doi.org/10.1038/s41585-024-00856-0
5. Avidor-Reiss T, Carr A, Fishman EL (2020) The sperm centrioles. Mol Cell Endocrinol 518:110987. https://doi.org/10.1016/j.mce.2020.110987
6. Bizkarguenaga M, Gomez-Santos L, Madrid JF et al (2022) Zona Pellucida sperm-binding protein 3 receptor distribution during Gopc(-/-) globozoospermic spermatogenesis. Microsc Res Tech 85:1454–1464. https://doi.org/10.1002/jemt.24009
7. Blaurock J, Baumann S, Grunewald S et al (2022) Metabolomics of human semen: a review of different Analytical methods to unravel biomarkers for Male Fertility disorders. Int J Mol Sci 23. https://doi.org/10.3390/ijms23169031
8. Bornens M (2012) The centrosome in cells and organisms. Science 335:422–426. https://doi.org/10.1126/science.1209037
9. Brukman NG, Nakajima KP, Valansi C et al (2023) A novel function for the sperm adhesion protein IZUMO1 in cell-cell fusion. J Cell Biol 222. https://doi.org/10.1083/jcb.202207147
10. Carvalho-Santos Z, Machado P, Alvarez-Martins I et al (2012) BLD10/CEP135 is a microtubule-associated protein that controls the formation of the flagellum central microtubule pair. Dev Cell 23:412–424. https://doi.org/10.1016/j.devcel.2012.06.001
11. Cong J, Wang X, Amiri-Yekta A et al (2022) Homozygous mutations in CCDC34 cause male infertility with oligoasthenoteratozoospermia in humans and mice. J Med Genet 59:710–718. https://doi.org/10.1136/jmedgenet-2021-107919
12. Crapster JA, Rack PG, Hellmann ZJ et al (2020) HIPK4 is essential for murine spermiogenesis. Elife 9. https://doi.org/10.7554/eLife.50209
13. Dahl KD, Sankaran DG, Bayless BA et al (2015) A short CEP135 splice isoform controls Centriole Duplication. Curr Biol 25:2591–2596. https://doi.org/10.1016/j.cub.2015.08.039
14. Dai J, Li Q, Zhou Q et al (2022) IQCN disruption causes fertilization failure and male infertility due to manchette assembly defect. EMBO Mol Med 14:e16501. https://doi.org/10.15252/emmm.202216501
15. Di Persio S, Tekath T, Siebert-Kuss LM et al (2021) Single-cell RNA-seq unravels alterations of the human spermatogonial stem cell compartment in patients with impaired spermatogenesis. Cell Rep Med 2:100395. https://doi.org/10.1016/j.xcrm.2021.100395
16. Fishman EL, Jo K, Nguyen QPH et al (2018) A novel atypical sperm centriole is functional during human fertilization. Nat Commun 9:2210. https://doi.org/10.1038/s41467-018-04678-8
17. Floriot S, Bellutti L, Castille J et al (2021) CEP250 is required for maintaining centrosome cohesion in the germline and fertility in male mice. Front Cell Dev Biol 9:754054. https://doi.org/10.3389/fcell.2021.754054
18. Ganapathi Sankaran D, Stemm-Wolf AJ, Pearson CG (2019) CEP135 isoform dysregulation promotes centrosome amplification in breast cancer cells. Mol Biol Cell 30:1230–1244. https://doi.org/10.1091/mbc.E18-10-0674
19. Geyer CB, Inselman AL, Sunman JA et al (2009) A missense mutation in the Capza3 gene and disruption of F-actin organization in spermatids of repro32 infertile male mice. Dev Biol 330:142–152. https://doi.org/10.1016/j.ydbio.2009.03.020
20. Gunes S, Esteves SC (2021) Role of genetics and epigenetics in male infertility. Andrologia 53:e13586. https://doi.org/10.1111/and.13586
21. Guo J, He WB, Dai L et al (2023) Mosaic variegated aneuploidy syndrome with tetraploid, and predisposition to male infertility triggered by mutant CEP192. HGG Adv 5:100256. https://doi.org/10.1016/j.xhgg.2023.100256
22. Hall EA, Keighren M, Ford MJ et al (2013) Acute versus chronic loss of mammalian Azi1/Cep131 results in distinct ciliary phenotypes. PLoS Genet 9:e1003928. https://doi.org/10.1371/journal.pgen.1003928
23. Hoque M, Chen D, Hess RA et al (2021) CEP164 is essential for efferent duct multiciliogenesis and male fertility. Reproduction 162:129–139. https://doi.org/10.1530/REP-21-0042
24. Hu T, Meng L, Tan C et al (2023) Biallelic CFAP61 variants cause male infertility in humans and mice with severe oligoasthenoteratozoospermia. J Med Genet 60:144–153. https://doi.org/10.1136/jmedgenet-2021-108249
25. Hua J, Xu B, Liu W et al (2023) Homozygous frameshift variant in POC1B causes male infertility with oligoasthenoteratozoospermia in human and mice. Hum Mol Genet 32:2307–2317. https://doi.org/10.1093/hmg/ddad061
26. Hussain MS, Baig SM, Neumann S et al (2012) A truncating mutation of CEP135 causes primary microcephaly and disturbed centrosomal function. Am J Hum Genet 90:871–878. https://doi.org/10.1016/j.ajhg.2012.03.016
27. Inanc B, Putz M, Lalor P et al (2013) Abnormal centrosomal structure and duplication in Cep135-deficient vertebrate cells. Mol Biol Cell 24:2645–2654. https://doi.org/10.1091/mbc.E13-03-0149
28. Jaiswal S, Singh P (2021) Centrosome dysfunction in human diseases. Semin Cell Dev Biol 110:113–122. https://doi.org/10.1016/j.semcdb.2020.04.019
29. Jin HJ, Ruan T, Dai S et al (2023) Identification of CFAP52 as a novel diagnostic target of male infertility with defects of sperm head-tail connection and flagella development. Elife 12. https://doi.org/10.7554/eLife.92769
30. Jin HJ, Wang JL, Geng XY et al (2023) CFAP70 is a solid and valuable target for the genetic diagnosis of oligo-astheno-teratozoospermia in infertile men. EBioMedicine 93:104675. https://doi.org/10.1016/j.ebiom.2023.104675
31. Kleylein-Sohn J, Westendorf J, Le Clech M et al (2007) Plk4-induced centriole biogenesis in human cells. Dev Cell 13:190–202. https://doi.org/10.1016/j.devcel.2007.07.002
32. Kraatz S, Guichard P, Obbineni JM et al (2016) The human centriolar protein CEP135 contains a two-stranded coiled-Coil Domain critical for Microtubule binding. Structure 24:1358–1371. https://doi.org/10.1016/j.str.2016.06.011
33. Krausz C, Riera-Escamilla A (2018) Genetics of male infertility. Nat Rev Urol 15:369–384. https://doi.org/10.1038/s41585-018-0003-3
34. Li YF, He W, Kim YH et al (2010) CABYR isoforms expressed in late steps of spermiogenesis bind with AKAPs and ropporin in mouse sperm fibrous sheath. Reprod Biol Endocrinol 8:101. https://doi.org/10.1186/1477-7827-8-101
35. Liang Z, Dai C, He F et al (2024) AKAP3-mediated type I PKA signaling is required for mouse sperm hyperactivation and fertilitydagger. Biol Reprod 110:684–697. https://doi.org/10.1093/biolre/ioad180
36. Lipshultz LI, Lamb DJ (2007) Risk of transmission of genetic diseases by assisted reproduction. Nat Clin Pract Urol 4:460–461. https://doi.org/10.1038/ncpuro0879
37. Liu Q, Guo Q, Guo W et al (2021) Loss of CEP70 function affects acrosome biogenesis and flagella formation during

spermiogenesis. Cell Death Dis 12:478. https://doi.org/10.1038/s41419-021-03755-z
38. Marjanovic M, Sanchez-Huertas C, Terre B et al (2015) CEP63 deficiency promotes p53-dependent microcephaly and reveals a role for the centrosome in meiotic recombination. Nat Commun 6:7676. https://doi.org/10.1038/ncomms8676
39. Marthiens V, Rujano MA, Pennetier C et al (2013) Centrosome amplification causes microcephaly. Nat Cell Biol 15:731–740. https://doi.org/10.1038/ncb2746
40. Martins AD, Majzoub A, Agawal A (2019) Metabolic syndrome and male fertility. World J Mens Health 37:113–127. https://doi.org/10.5534/wjmh.180055
41. Matzuk MM, Lamb DJ (2008) The biology of infertility: research advances and clinical challenges. Nat Med 14:1197–1213. https://doi.org/10.1038/nm.f.1895
42. Mima M, Greenwald D, Ohlander S (2018) Environmental toxins and male fertility. Curr Urol Rep 19:50. https://doi.org/10.1007/s11934-018-0804-1
43. Panner Selvam MK, Agarwal A, Henkel R et al (2020) The effect of oxidative and reductive stress on semen parameters and functions of physiologically normal human spermatozoa. Free Radic Biol Med 152:375–385. https://doi.org/10.1016/j.freeradbiomed.2020.03.008
44. Ray PF, Toure A, Metzler-Guillemain C et al (2017) Genetic abnormalities leading to qualitative defects of sperm morphology or function. Clin Genet 91:217–232. https://doi.org/10.1111/cge.12905
45. Remo A, Li X, Schiebel E et al (2020) The Centrosome Linker and its role in Cancer and Genetic disorders. Trends Mol Med 26:380–393. https://doi.org/10.1016/j.molmed.2020.01.011
46. Ruan T, Yang Y, Jiang C et al (2023) Identification of biallelic variations of CEP70 in patients with male infertility. Front Endocrinol (Lausanne) 14:1133222. https://doi.org/10.3389/fendo.2023.1133222
47. Salicioni AM, Gervasi MG, Sosnik J et al (2020) Testis-specific serine kinase protein family in male fertility and as targets for non-hormonal male contraceptiondagger. Biol Reprod 103:264–274. https://doi.org/10.1093/biolre/ioaa064
48. Sengupta P, Roychoudhury S, Nath M et al (2022) Oxidative stress and idiopathic male infertility. Adv Exp Med Biol 1358:181–204. https://doi.org/10.1007/978-3-030-89340-8_9
49. Sha YW, Xu X, Mei LB et al (2017) A homozygous CEP135 mutation is associated with multiple morphological abnormalities of the sperm flagella (MMAF). Gene 633:48–53. https://doi.org/10.1016/j.gene.2017.08.033
50. Shen Y, Zhang F, Li F et al (2019) Loss-of-function mutations in QRICH2 cause male infertility with multiple morphological abnormalities of the sperm flagella. Nat Commun 10:433. https://doi.org/10.1038/s41467-018-08182-x
51. Sinha D, Kalimutho M, Bowles J et al (2018) Cep55 overexpression causes male-specific sterility in mice by suppressing Foxo1 nuclear retention through sustained activation of PI3K/Akt signaling. FASEB J 32:4984–4999. https://doi.org/10.1096/fj.201701096RR
52. Tardif S, Akrofi AS, Dass B et al (2010) Infertility with impaired zona pellucida adhesion of spermatozoa from mice lacking TauC-stF-64. Biol Reprod 83:464–472. https://doi.org/10.1095/biolreprod.109.083238
53. Thonneau P, Marchand S, Tallec A et al (1991) Incidence and main causes of infertility in a resident population (1,850,000) of three French regions (1988–1989). Hum Reprod 6:811–816. https://doi.org/10.1093/oxfordjournals.humrep.a137433
54. Turner KA, Caswell DL, Mcgrady BM et al (2023) CP110 and CEP135 localize near the proximal and distal centrioles of cattle and human spermatozoa. MicroPubl Biol 2023. https://doi.org/10.17912/micropub.biology.000951
55. Tuttelmann F, Ruckert C, Ropke A (2018) Disorders of spermatogenesis: perspectives for novel genetic diagnostics after 20 years of unchanged routine. Med Genet 30:12–20. https://doi.org/10.1007/s11825-018-0181-7
56. Umer N, Phadke S, Shakeri F et al (2022) PFN4 is required for manchette development and acrosome biogenesis during mouse spermiogenesis. Development 149. https://doi.org/10.1242/dev.200499
57. Wang X, Wei Y, Fu G et al (2015) Tssk4 is essential for maintaining the structural integrity of sperm flagellum. Mol Hum Reprod 21:136–145. https://doi.org/10.1093/molehr/gau097
58. Weidemann M, Schuster-Gossler K, Stauber M et al (2016) CFAP157 is a murine downstream effector of FOXJ1 that is specifically required for flagellum morphogenesis and sperm motility. Development 143:4736–4748. https://doi.org/10.1242/dev.139626
59. Wu B, Gao H, Liu C et al (2020) The coupling apparatus of the sperm head and taildagger. Biol Reprod 102:988–998. https://doi.org/10.1093/biolre/ioaa016
60. Wyrwoll MJ, Van Der Heijden GW, Krausz C et al (2024) Improved phenotypic classification of male infertility to promote discovery of genetic causes. Nat Rev Urol 21:91–101. https://doi.org/10.1038/s41585-023-00816-0
61. Xu K, Yang L, Zhang L et al (2020) Lack of AKAP3 disrupts integrity of the subcellular structure and proteome of mouse sperm and causes male sterility. Development 147. https://doi.org/10.1242/dev.181057
62. Yamatoya K, Kousaka M, Ito C et al (2020) Cleavage of SPACA1 regulates assembly of sperm-egg membrane fusion machinery in mature spermatozoadagger. Biol Reprod 102:750–757. https://doi.org/10.1093/biolre/ioz223
63. Yuan S, Stratton CJ, Bao J et al (2015) Spata6 is required for normal assembly of the sperm connecting piece and tight head-tail conjunction. Proc Natl Acad Sci U S A 112:E430–439. https://doi.org/10.1073/pnas.1424648112
64. Zegers-Hochschild F, Adamson GD, Dyer S et al (2017) The International Glossary on Infertility and Fertility Care, 2017. Fertil Steril 108:393–406. https://doi.org/10.1016/j.fertnstert.2017.06.005
65. Zhang Y, Liu C, Wu B et al (2021) The missing linker between SUN5 and PMFBP1 in sperm head-tail coupling apparatus. Nat Commun 12:4926. https://doi.org/10.1038/s41467-021-25227-w
66. Zhang X, Wang L, Ma Y et al (2022) CEP128 is involved in spermatogenesis in humans and mice. Nat Commun 13:1395. https://doi.org/10.1038/s41467-022-29109-7
67. Zhang X, Zheng R, Liang C et al (2022) Loss-of-function mutations in CEP78 cause male infertility in humans and mice. Sci Adv 8:eabn0968. https://doi.org/10.1126/sciadv.abn0968
68. Zheng H, Gong C, Li J et al (2024) CCDC157 is essential for sperm differentiation and shows oligoasthenoteratozoospermia-related mutations in men. J Cell Mol Med 28:e18215. https://doi.org/10.1111/jcmm.18215
69. Zhou D, Wu H, Wang L et al (2024) Deficiency of MFSD6L, an acrosome membrane protein, causes oligoasthenoteratozoospermia in humans and mice. J Genet Genomics. https://doi.org/10.1016/j.jgg.2024.06.008
70. Zhu T, Zhang Y, Sheng X et al (2023) Absence of CEP78 causes photoreceptor and sperm flagella impairments in mice and a human individual. Elife 12. https://doi.org/10.7554/eLife.76157